LBL-32309
UC-413
Preprint

Lawrence Berkeley Laboratory
UNIVERSITY OF CALIFORNIA

Submitted to Annals of Physics

Spin-Orbit Coupling in Semiclassical Approximation

H. Frisk and T. Guhr

May 1992

LOAN COPY
Circulates
for 4 weeks
Bldg. 50 Library.
LBL-32309
Copy 2

Prepared for the U.S. Department of Energy under Contract Number DE-AC03-76SF00098

DISCLAIMER

This document was prepared as an account of work sponsored by the United States Government. Neither the United States Government nor any agency thereof, nor The Regents of the University of California, nor any of their employees, makes any warranty, express or implied, or assumes any legal liability or responsibility for the accuracy, completeness, or usefulness of any information, apparatus, product, or process disclosed, or represents that its use would not infringe privately owned rights. Reference herein to any specific commercial product, process, or service by its trade name, trademark, manufacturer, or otherwise, does not necessarily constitute or imply its endorsement, recommendation, or favoring by the United States Government or any agency thereof, or The Regents of the University of California. The views and opinions of authors expressed herein do not necessarily state or reflect those of the United States Government or any agency thereof or The Regents of the University of California and shall not be used for advertising or product endorsement purposes.

Lawrence Berkeley Laboratory is an equal opportunity employer.

DISCLAIMER

This document was prepared as an account of work sponsored by the United States Government. While this document is believed to contain correct information, neither the United States Government nor any agency thereof, nor the Regents of the University of California, nor any of their employees, makes any warranty, express or implied, or assumes any legal responsibility for the accuracy, completeness, or usefulness of any information, apparatus, product, or process disclosed, or represents that its use would not infringe privately owned rights. Reference herein to any specific commercial product, process, or service by its trade name, trademark, manufacturer, or otherwise, does not necessarily constitute or imply its endorsement, recommendation, or favoring by the United States Government or any agency thereof, or the Regents of the University of California. The views and opinions of authors expressed herein do not necessarily state or reflect those of the United States Government or any agency thereof or the Regents of the University of California.

LBL-32309

Spin-Orbit Coupling in Semiclassical Approximation*

Hans Frisk[1,2] and Thomas Guhr[1]
[1]Lawrence Berkeley Laboratory
University of California
Berkeley, CA 94720, USA
[2]NORDITA, Blegdamsvej 17
2100 Copenhagen Ø, Denmark

May 15, 1992

Abstract

The spin-orbit coupling in a deformed system is studied by approximating the Schrödinger equation semiclassically. The discrete character of spin is preserved and WKB techniques are used for the coupled two-component wave equations. Thus, contrary to other approaches, spin is not treated similar to a classical angular momentum. Information about the periodic orbits is extracted from Fourier transforms of the quantum mechanical spectra and compared to classical calculations. Planar motion exhibiting mode conversion and non-planar motion, for which Berry's phase is important, are investigated. For planar orbits, the semiclassical method is successfully corrected for mode conversion.

*This work was supported by the Director, Office of Energy Research, Office of High Energy and Nuclear Physics, Division of Nuclear Physics, of the U.S. Department of Energy under Contract DE-AC03-76SF00098

1 Introduction

In quantum mechanics, the physical concept of spin is well incorporated into the theory, at least from a technical viewpoint. The spin and its $SU(2)$ character are inherent properties of the Dirac equation. In the presence of electromagnetic couplings a nonrelativistic approximation of the Dirac equation gives to lowest order the two-component Pauli equation and the spin-orbit interaction appears in next order [1]. Alternatively, the spin-orbit coupling appears in the adiabatic effective Hamiltonian for the orbital motion of the Dirac particle [2]. The original motivation for a spin-orbit term in the nuclear case was phenomenological. As well known, the inclusion of this term was a crucial step in the development of the nuclear shell model [3, 4]. However, nucleons are not point Dirac particles and therefore the microscopical description of the spin-orbit interaction is a complex issue [5].

On the other hand, a direct and obvious classical anology of spin is lacking. Spin correlation experiments show highly non-classical features [6] and it is thus not clear what aspects of spin are relevant in a classical model. The most nearlying classical picture for the concept of a quantum particle with spin is the motion of a top or a gyroscope with an intrinsic angular momentum besides the orbital one. In other words, the $SU(2)$ spin is interpreted as an $SO(3)$ angular momentum. This gives indeed for many aspects a very instructive picture, for a detailed review see Corben's book [7]. A way to justify this replacement of a quantal concept by a classical one is to derive classical equations of motion by a variational principle using coherent state wave functions [8]. This gives a classical model with two additional angles and two conjugate momenta in the classical phase space whereas the length of this intrinsic angular momentum is fixed [8, 9].

However, in this paper we abandon the $SO(3)$ picture and go a different way. The Schrödinger equation for a spinor wave function is nothing else but a system of coupled wave equations whose semiclassical approximation has to be found. Thus, we preserve the discrete nature of spin and treat only the orbital motion semiclassically. The merit of this method is that no extended phase space is needed, the effect of spin is just an additional force on the orbital motion. The mathematical tool that we need, the Wentzel-Kramers-Brillouin (WKB) theory for multicomponent wave equations, has been worked out by Yabana and Horiuchi [10] in the one dimensional case. This theory is essentially an adiabatic approximation which in our case means

that the orbital motion is assumed to be much slower than the spin motion. Besides Berry's phase [11] an additional phase correction to the WKB wave function was found in reference [10]. This theory has recently been considerably improved and extended to arbitrary dimensions by Littlejohn and Flynn who used the Weyl symbol calculus [12]. In the course of our work we discovered that our approach is in the spirit of early, brief considerations by Balian and Bloch [13]. As an application of the improved WKB theory Littlejohn and Flynn have in great detail investigated the case of spin-orbit coupling in spherical potentials [14]. Here, we focus attention on spin-orbit interaction in deformed systems for which the atomic nuclei provide an obvious physical motivation [4]. The deformation causes interesting new effects which are not present in the spherical case. For example, diabatic transitions between spin polarizations, in the following called mode conversion, take place and are associated with the breakdown of the WKB theory.

In our investigations we rely on the theory of trace formulas as first developed by Gutzwiller [15] and later by Balian and Bloch [16] and Berry and Tabor [17]. The trace of the semiclassical Green function expresses the density of eigenenergies for a bound quantal system as a sum over the periodic orbits in the corresponding classical system. It is the only tool available for semiclassical quantization of chaotic systems [15]. If only the smooth oscillations of the level density are of interest, as for example in shell structure calculations, the shortest periodic orbits give very accurate and valuable information [18, 19]. Despite severe difficulties with the inclusion of the long periodic orbits progress has been made recently [20]. However, the perspective for a periodic orbit formula for the eigenstates [21] is not bright since numerical results strongly call for an improvement of the present theory [22]. Much of the work in this field has dealt with fermions but until recently only little attention has been paid to the problem of incorporating spin into the formalism, except for the work of Balian and Bloch [13] mentioned above. The starting point for Gutzwiller's semiclassical approximations is the path integral, where, in the original formulation, spin was not included in a convincing way [23]. Schulman was the first to make real progress [24]. In the framework of a gyroscope like picture, he quantized the spherical top and used the freedom to choose the relative phase factor between paths belonging to the two homotopy classes to obtain half-integer spin. However, such models with additional intrinsic degrees of freedom like $SO(3)$ are difficult to extend to a quantized relativistic theory. For that reason an alternative

approach was developed by Polyakov [25]. He realized that the effect of spin can be incorporated by a weight, or spin factor, attached to each path and that this weight depends only on the geometrical properties of the path itself. This weight is related to a Berry's phase [26]. Thus, the focus is here on the influence of the spin on the geometry of the paths and no intrinsic structure of the particle is assumed. Our approach is obviously in the same spirit.

We would like to emphasize that our investigation although motivated by nuclear physics is more the object of a general discussion to shed light on the role of the spin in semiclassical theories. At this stage we do not intend to perform quantitative nuclear structure calculations. However, in rotating nuclei with extreme, superdeformed shapes an integer, or half-integer, quantization of the rotational angular momentum has been reported recently [27]. This remarkable observation encourages a careful study of the spin properties in these systems. Hence, at a further stage, our approach might be of some relevance in concrete applications.

We tried to write this paper in a readable form also for those with little background in semiclassical physics. Thus, section 2 is a detailed selfcontained presentation of our model and the procedures we use. To test our approach, we perform classical and quantal numerical calculations as well, the results are compared in section 3. We discuss our findings in section 4. Two special calculations are shifted into the appendix.

2 Semiclassical Theory and Procedure

After formulating the problem in subsection 2.1, we give a brief summary of the WKB methods in subsection 2.2 and apply these to our system in subsection 2.3. In subsection 2.4 we choose the potential, thereby constructing a scaling system. The Fourier transform technique which is our tool to analyze the quantal calculations is discussed in subsection 2.5.

2.1 Formulation of the Problem

The time independent Schrödinger equation for a particle with spin that is described by a two component spinor wave function ψ can be written in the form

$$\underset{\sim}{D}\,\psi \;=\; 0 \qquad \text{where} \qquad \underset{\sim}{D} \;=\; \underset{\sim}{H} - E\underset{\sim}{1} \tag{1}$$

is interpreted as a dispersion tensor, $\underset{\sim}{H}$ is the Hamiltonian operator and E the energy. Here and in the following, variables underlined with $\underset{\sim}{\ }$ are quantum mechanical operators. In a deformed mean field potential $V(\underset{\sim}{\vec{r}})$ the Hamiltonian including an interaction between orbit and spin $\underset{\sim}{\vec{S}}$ is given by

$$\begin{aligned} \underset{\sim}{H} &= \frac{1}{2m}\underset{\sim}{\vec{p}}^2 + V(\underset{\sim}{\vec{r}}) - 2\kappa\, \underset{\sim}{\vec{B}} \cdot \underset{\sim}{\vec{S}} \\ \underset{\sim}{\vec{B}} &= \frac{\partial V_{so}}{\partial \vec{r}}(\underset{\sim}{\vec{r}}) \times \underset{\sim}{\vec{p}} \quad . \end{aligned} \tag{2}$$

The form of $\underset{\sim}{\vec{B}}$ is the simplest possible for a pseudovector assuming a coupling proportional to a gradient of a potential [4]. The function $V_{so}(\underset{\sim}{\vec{r}})$ is called spin-orbit potential and 2κ is an adjustable spin-orbit parameter. The usual choice is $V_{so}(\underset{\sim}{\vec{r}}) = V(\underset{\sim}{\vec{r}})$, but in the nuclear case the two potentials can take different forms [28], of course, the deformation should be the same. In the spherical case we find the familiar expression

$$\underset{\sim}{\vec{B}} = \frac{1}{\underset{\sim}{r}} \frac{dV_{so}}{dr}(\underset{\sim}{r})\, \underset{\sim}{\vec{L}} \qquad \text{if} \qquad V_{so}(\underset{\sim}{\vec{r}}) = V_{so}(\underset{\sim}{r}) \tag{3}$$

where $\underset{\sim}{\vec{L}} = \underset{\sim}{\vec{r}} \times \underset{\sim}{\vec{p}}$ is the angular momentum operator.

The components of the spin vector $\underset{\sim}{\vec{S}}$ are one half times the Pauli spin matrices, hence we arrive at a 2×2 matrix representation of the dispersion tensor

$$\underset{\sim}{D} = \left(\frac{1}{2m}\underset{\sim}{\vec{p}}^2 + V(\underset{\sim}{\vec{r}}) - E\underset{\sim}{1}\right) 1_2 - \kappa \begin{bmatrix} \underset{\sim}{B}_z & \underset{\sim}{B}_- \\ \underset{\sim}{B}_+ & -\underset{\sim}{B}_z \end{bmatrix} \tag{4}$$

where 1_2 is the 2×2 unit matrix and $\underset{\sim}{B}_\pm = \underset{\sim}{B}_x \pm i\underset{\sim}{B}_y$.

We are aiming now at a semiclassical solution of the Schrödinger equation (1), i.e. of a two component coupled wave equation, with $\underset{\sim}{D}$ given by (4). In order to achieve this goal we apply the powerful method of Littlejohn and Flynn [12]. In the following subsection, we briefly sketch the main ideas, presentation and notation follow closely reference [12].

2.2 WKB for Multicomponent Wave Equations

A wave equation of type (1) with an, in general, M-component spinor ψ and an $M \times M$ dispersion tensor $\underset{\sim}{D}$ is not easily eligible for semiclassical

methods, since it is actually a coupled system of M equations. However, if $\underset{\sim}{D}$ is Hermitean, those can be decoupled by diagonalization. Hence, we require the existence of an unitary matrix $\underset{\sim}{U}$ with the property

$$\underset{\sim}{U}^\dagger \underset{\sim}{D} \underset{\sim}{U} \;=\; \underset{\sim}{\Lambda} \qquad \text{where} \qquad \underset{\sim}{\Lambda} \;=\; \mathrm{diag}(\underset{\sim}{\lambda}_1, \ldots, \underset{\sim}{\lambda}_M) \quad . \tag{5}$$

This yields M decoupled equations because $\underset{\sim}{\Lambda}$ is diagonal,

$$\underset{\sim}{\Lambda}\,\varphi \;=\; 0 \qquad \text{where} \qquad \varphi \;=\underset{\sim}{U}^\dagger \psi \quad . \tag{6}$$

These equations can now be analysed with standard scalar WKB methods [29]. Unfortunately, the diagonalization is highly nontrivial since the elements of $\underset{\sim}{D}$ are operators. The Weyl symbol calculus, however, provides a tool to solve this problem by an expansion [12]. The Weyl symbol of an operator $\underset{\sim}{A}$ is the phase-space function [30]

$$A_W(\vec{r},\vec{p}) \;=\; \int d^3q \, \exp\left(-\frac{i}{\hbar}\vec{q}\cdot\vec{p}\right) \langle \vec{r}+\vec{q}/2|\underset{\sim}{A}|\vec{r}-\vec{q}/2\rangle \quad , \tag{7}$$

i.e., the Wigner-transform. The symbol of the product of two operators $\underset{\sim}{A}$ and $\underset{\sim}{B}$ is given by the Moyal-formula [30]

$$(\underset{\sim}{A}\underset{\sim}{B})_W(\vec{r},\vec{p}) \;=\; A_W(\vec{r},\vec{p}) \exp\left(i\frac{\hbar}{2}\left(\frac{\overleftarrow{\partial}}{\partial\vec{r}}\frac{\overrightarrow{\partial}}{\partial\vec{p}} - \frac{\overleftarrow{\partial}}{\partial\vec{p}}\frac{\overrightarrow{\partial}}{\partial\vec{r}}\right)\right) B_W(\vec{r},\vec{p}) \tag{8}$$

implying the following relation between the quantum mechanical commutator $[,]$ and the classical Poisson-brackets $\{,\}$

$$[\underset{\sim}{A},\underset{\sim}{B}]_W(\vec{r},\vec{p}) \;=\; i\hbar\,\{A_W(\vec{r},\vec{p}), B_W(\vec{r},\vec{p})\} \;+\; \mathcal{O}(\hbar^2) \tag{9}$$

The first order approximation is reasonable if $A_W(\vec{r},\vec{p})$ and $B_W(\vec{r},\vec{p})$ are slowly varying functions on phase space. In the following the subscript W will be omitted from the Weyl symbol and we write $A(\vec{r},\vec{p})$ instead of $A_W(\vec{r},\vec{p})$.

To obtain the Weyl symbol corresponding to equation (5) one introduces the following ansatz as power series in $\hbar$,

$$X(\vec{r},\vec{p}) \;=\; \sum_{n=0}^{\infty} \hbar^n \, X^{(n)}(\vec{r},\vec{p}) \tag{10}$$

where X stands for either of the symbol matrices U and Λ. To be more precise, the true expansion parameter is $\hbar/S_0$ where S_0 is a typical action of the system. By employing the unitarity condition on the diagonalizing matrix and the Moyal formula this ansatz yields systems of equations for each power of $\hbar$. In zeroth order we have

$$\Lambda^{(0)}(\vec{r},\vec{p}) \;=\; U^{(0)\dagger}(\vec{r},\vec{p})\, D(\vec{r},\vec{p})\, U^{(0)}(\vec{r},\vec{p}) \quad . \tag{11}$$

The eigenvectors to the eigenvalue $\lambda_\mu^{(0)}(\vec{r},\vec{p})$, i.e.

$$\tau_\alpha^{(\mu)}(\vec{r},\vec{p}) \;=\; U_{\alpha\mu}^{(0)}(\vec{r},\vec{p}) \quad , \qquad \mu \;=\; 1,\ldots,M \tag{12}$$

are called polarization vectors and μ is the polarization index. Up to first order in $\hbar$ we have

$$\Lambda(\vec{r},\vec{p}) \;=\; \Lambda^{(0)}(\vec{r},\vec{p}) \;+\; \hbar\Lambda^{(1)}(\vec{r},\vec{p}) \quad . \tag{13}$$

The first order term is a sum of two contributions

$$\Lambda^{(1)}(\vec{r},\vec{p}) \;=\; \Lambda^{(1\mathrm{B})}(\vec{r},\vec{p}) \;+\; \Lambda^{(1\mathrm{NN})}(\vec{r},\vec{p}) \tag{14}$$

whose components are given by

$$\begin{aligned}
\lambda_\mu^{(1\mathrm{B})} &= -i\sum_{\alpha=1}^{M} \tau_\alpha^{(\mu)\star}\,\{\tau_\alpha^{(\mu)},\lambda_\mu^{(0)}\} \;=\; -i\sum_{\alpha=1}^{M} \tau_\alpha^{(\mu)\star}\,\frac{d\tau_\alpha^{(\mu)}}{dt} \\
\lambda_\mu^{(1\mathrm{NN})} &= -\frac{i}{2}\sum_{\alpha,\beta}(D_{\alpha\beta}-\lambda_\mu^{(0)}\delta_{\alpha\beta})\,\{\tau_\alpha^{(\mu)\star},\tau_\beta^{(\mu)}\} \quad .
\end{aligned} \tag{15}$$

The first of these we call Berry's contribution since it is associated with Berry's phase [11]. It often appears when a system is divided into "slow" and "fast" parts as in the Born-Oppenheimer treatment of molecules. Here it is assumed that the orbital and spin degrees of freedom can be treated separately. The second term is sometimes called the "no name" contribution and therefore labeled NN. It vanishes if the polarization vector depends only on $\vec{r}$ or $\vec{p}$. Note that the Poisson bracket appearing in Berry's contribution can be written as a time derivative since $\lambda_\mu^{(0)}$ is the zeroth order Hamiltonian up to a constant.

Besides the condition that the Weyl symbols are slowly varying functions on phase space one must exclude degeneracies of the eigenvalues of the symbol

matrix $D(\vec{r},\vec{p})$ to make the procedure meaningful [12]. Those lead to mode conversion points and we will have to deal with them in our application. The decoupled wave equations are now eligible to the standard WKB analysis. Since Hamilton's equations can be formulated as a variational principle on phase space we have the following M conditions, one for each eigenvalue

$$\delta \int \left(\vec{p} \cdot d\vec{r} - \left(\lambda_\mu^{(0)} + \hbar \left(\lambda_\mu^{(1B)} + \lambda_\mu^{(1NN)} \right) \right) dt \right) = 0 \quad . \tag{16}$$

Some problems arise since the total WKB wave function has to be invariant under gauge transformations $\tau^{(\mu)}(\vec{r},\vec{p}) \rightarrow \tau^{(\mu)}(\vec{r},\vec{p}) \exp(i\Theta(\vec{r},\vec{p}))$ where $\Theta(\vec{r},\vec{p})$ is the gauge function. It turns out that the "no name" part $\lambda_\mu^{(1NN)}$ is invariant under those transformations whereas Berry's part transforms as $\lambda_\mu^{(1B)} \rightarrow \lambda_\mu^{(1B)} + \{\Theta, \lambda_\mu^{(0)}\}$. In order to remedy this problem new non-canonical coordinates $(\vec{r}\,',\vec{p}\,')$ are introduced [12] in such a way that Berry's contribution is absorbed in the symplectic form $\vec{p}\,' \cdot d\vec{r}\,'$ where it gives rise to Berry's phase [11]. To first order in $\hbar$, the new equations of motion have the form

$$\begin{aligned} \frac{d}{dt} \begin{bmatrix} \vec{r}\,' \\ \vec{p}\,' \end{bmatrix} &= J \frac{\partial}{\partial(\vec{r}\,',\vec{p}\,')} \left(\lambda_\mu^{(0)} + \hbar \lambda_\mu^{(1NN)} \right) \\ J &= \begin{bmatrix} 0 & 1_3 \\ -1_3 & 0 \end{bmatrix} + \hbar J^{(1)} \quad . \end{aligned} \tag{17}$$

The 6×6 matrix $J^{(1)}$ vanishes in the case of canonical coordinates. In their one dimensional WKB theory for multicomponent wave fields, Yabana and Horiuchi [10] include also $\hbar\lambda_\mu^{(1NN)}$ in the symplectic form. Then only $\lambda_\mu^{(0)}$ is used as Hamiltonian in the equations of motion yielding a system similar to equations (17) but with a different $J^{(1)}$.

2.3 Application to the Spin-Orbit Problem

The symbol matrix $D(\vec{r},\vec{p})$ corresponding to the dispersion tensor (4) has the zeroth order eigenvalues

$$\begin{aligned} \lambda_\pm^{(0)}(\vec{r},\vec{p}) &= \frac{\vec{p}^{\,2}}{2m} + V(\vec{r}) \pm \kappa B - E \\ \vec{B} &= \frac{\partial V_{so}}{\partial \vec{r}}(\vec{r}) \times \vec{p} \end{aligned} \tag{18}$$

where $B = |\vec{B}|$. The polarization indices plus and minus correspond to the situations energetically unfavoured and favoured by the spin-orbit force, respectively. The relevant matrix structure of $D(\vec{r},\vec{p})$ is precisely the quaternion representation of the vector $\vec{B}$ implying that the diagonalizing matrix is only a function of its orientation $\vec{e}_B = \vec{B}/B$, i.e., $U = U(\vec{e}_B)$ and thus only an implicit function of the phase space coordinates $(\vec{r},\vec{p})$. Hence, the same is true for the polarization vectors, $\tau^{(\pm)} = \tau^{(\pm)}(\vec{e}_B)$. An underlying assumption in the semiclassical procedure presented above was that the symbol matrices are slowly varying functions on phase space. Since the relevant quantities for the diagonalization depend only on $\vec{e}_B$, this condition is fulfilled if $\vec{B}$ moves slowly. Our semiclassical WKB-analysis is in that sense an adiabatic approximation. However, a special situation occurs if the momentum $\vec{p}$ and the gradient of the spin orbit potential $\partial V_{\rm so}/\partial\vec{r}$ happen to be parallel or antiparallel. In that case, $\vec{B}$ vanishes. Equation (18) shows that at these points the eigenvalues $\lambda_\pm^{(0)}$ are degenerate which is equivalent to the total breakdown of the whole WKB treatment. These points are precisely the mode conversion points.

Berry's contribution is easily calculated by introducing spherical coordinates in $\vec{B}$-space, $\vec{e}_B = (\cos\varphi\sin\vartheta, \sin\varphi\sin\vartheta, \cos\vartheta)$,

$$\lambda_\pm^{(1\mathrm{B})} = \mp\frac{1}{2}(1-\cos\vartheta)\,\dot{\varphi} \tag{19}$$

where we chose the north standard gauge, see appendix. The gauge independent "no name" contribution is given by

$$\lambda_\pm^{(1\mathrm{NN})} = \frac{\kappa}{2}\,\vec{e}_B^{\,T}\,\frac{\partial^2 V_{\rm so}}{\partial\vec{r}\,\partial\vec{r}^{\,T}}\,\vec{e}_B \quad , \tag{20}$$

the somewhat lengthy calculation is briefly sketched in the appendix. It is worthwhile to emphasize that both first order contributions depend only on the direction of $\vec{B}$ but not on its magnitude. Moreover, they only implicitly depend on the mean field potential $V(\vec{r})$.

It is very instructive to consider the spherical case $V_{\rm so}(\vec{r}) = V_{\rm so}(r)$ for a moment. We have

$$\vec{B} = \frac{1}{r}\frac{dV_{\rm so}}{dr}(r)\,\vec{L} \qquad \text{where} \qquad \vec{L} = \vec{r}\times\vec{p} \tag{21}$$

is the angular momentum. Since $\vec{L}$ is now a constant of motion Berry's contribution vanishes in any gauge. The matrix of the double derivatives is given by

$$\frac{\partial^2 V_{\rm so}(r)}{\partial\vec{r}\,\partial\vec{r}^{\,T}} = \left(\frac{d^2V_{\rm so}}{dr^2}(r) - \frac{1}{r}\frac{dV_{\rm so}}{dr}\right)\vec{e}_r\,\vec{e}_r^{\,T} + \frac{1}{r}\frac{dV_{\rm so}}{dr}\,1_3 \tag{22}$$

with $\vec{e}_r = \vec{r}/r$. Since $\vec{L}\cdot\vec{r} = 0$ we find

$$\lambda_\pm^{(1\rm NN)} = \frac{\kappa}{2r}\frac{dV_{\rm so}}{dr}(r) \quad . \tag{23}$$

Only a first order derivative of the spin-orbit potential, precisely $\kappa/2$ times the radial function in the spin-orbit coupling term contributes. This is in perfect agreement with the analysis of the spherical problem by Littlejohn and Flynn [14]. Note that the exact result for the spin-orbit splitting is found by using the semiclassical quantization rule $L = \hbar(l+1/2)$, $l = 0,1,2,\ldots$,

$$\begin{aligned}\lambda_\pm + E &= \frac{\vec{p}^{\,2}}{2m} + V \pm \kappa\frac{1}{r}\frac{dV_{\rm so}}{dr}\hbar\left(l+\frac{1}{2}\right) + \hbar\frac{\kappa}{2r}\frac{dV_{\rm so}}{dr} \\ &= \frac{\vec{p}^{\,2}}{2m} + V + \frac{\hbar\kappa}{r}\frac{dV_{\rm so}}{dr}\begin{cases}-l & \text{favoured}\\ l+1 & \text{unfavoured}\end{cases} \quad .\end{aligned} \tag{24}$$

The reason for this agreement is the perfect fulfillment of the adiabaticity assumption since $\vec{e}_B$ is a constant of motion.

We now have to evaluate the equations of motion. Either of the two methods of dealing with the first order contributions to the eigenvalues of the dispersion tensor described at the end of the last subsection implies $\hbar$ corrections to the equations of motion. In our application, however, we assume that the coordinates can be chosen in such a way that these corrections are negligible. This leads us to the following recipe: *Use the zeroth order eigenvalue $\lambda_\pm^{(0)}$ as Hamiltonian in the canonical equations of motion and add the whole first order part $\hbar(\lambda_\pm^{(1\rm B)} + \lambda_\pm^{(1\rm NN)})\,dt$ to the symplectic form.* The possible marginal loss of accuracy in some of our results due to this recipe is not too serious a drawback since we are aiming more at a general and qualitative understanding of the semiclassical analysis of the spin-orbit problem and less at a quantitative one. Hence, for our purposes, the shortcomings due to this neglect of the first order corrections are certainly outweighted

by the advantage of having a clear and simple structure of the equations of motion.

Using this recipe, the two Hamiltonians are according to (18) given by

$$H(\vec{r},\vec{p}) \;=\; \frac{\vec{p}^{\,2}}{2m} + V(\vec{r}) - \kappa B \quad . \tag{25}$$

To simplify the notation, we dropped the polarization indices and the plus minus sign in front of κB. We allow κ to take positive and negative values and can thereby discuss both Hamiltonians at the same time. The equations of motion are

$$\begin{aligned} \dot{\vec{r}} &= +\frac{\partial H}{\partial \vec{p}} = \frac{\vec{p}}{m} + \kappa\,\frac{\partial V_{so}}{\partial \vec{r}} \times \vec{e}_B \\ \dot{\vec{p}} &= -\frac{\partial H}{\partial \vec{r}} = -\frac{\partial V}{\partial \vec{r}} + \kappa\,\frac{\partial^2 V_{so}}{\partial \vec{r}\,\partial \vec{r}^{\,T}}\,(\vec{p} \times \vec{e}_B) \quad . \end{aligned} \tag{26}$$

Again, only the direction of the vector $\vec{B}$ enters, not its magnitude.

2.4 Choice of Potentials and Scaling

All results derived so far are valid for sufficiently smooth but otherwise arbitrary, deformed potentials $V(\vec{r})$ and $V_{so}(\vec{r})$. In order to perform numerical calculations, we now have to specify them explicitly. Since our model system is motivated by nuclear physics, we choose an ellipsoidal deformation defined by the half axes $R_\perp$ in the (x,y) plane and R_z in the z-direction. For notational purposes we introduce the matrix $C = \mathrm{diag}(R_\perp^{-1}, R_\perp^{-1}, R_z^{-1})$. Only prolate shapes are considered such that the axis ratio $\mu = R_z/R_\perp$ is not less than unity. For normal deformed nuclei one has $\mu \simeq 1.2\ldots1.3$ while for superdeformed nuclei [4, 31] one finds $\mu \simeq 1.6\ldots2.0$. We define an average radius R_0 by the volume conserving condition $R_0^3 = R_\perp^2 R_z$ which yields $R_\perp = \mu^{-1/3}R_0$ and $R_z = \mu^{2/3}R_0$.

The next step is to choose the functional form of the potentials. As it is well known, scaling properties simplify numerical calculations tremendously. Such a scaling property can be achieved by choosing an infinite square well as mean field potential. Since $\vec{r}^{\,T}C^2\vec{r} = |C\vec{r}|^2 = 1$ describes the ellipsoid we set

$$V(\vec{r}) \;=\; \begin{cases} 0 & \text{if} \quad |C\vec{r}| < 1 \\ \infty & \text{if} \quad |C\vec{r}| \geq 1 \end{cases} \tag{27}$$

as a cavity with ideally reflecting boundary. The scaling transformation we have in mind is the simultaneous mapping

$$\vec{p} \longrightarrow \sigma \vec{p} \qquad \text{and} \qquad \kappa \longrightarrow \sigma \kappa \tag{28}$$

where σ is any real dimensionless number. From (25) and (27) we find that under this transformation the energy behaves as $E \rightarrow \sigma^2 E$. Hence the parameter

$$\eta = \frac{R_0^4}{m R_z^2} \frac{E}{\kappa^2} \tag{29}$$

is scaling invariant. The prefactors in this definition are choosen such that η is dimensionless. Thereby we made the spin-orbit potential $V_{so}(\vec{r})$ dimensionless by absorbing all strength constants into κ which now has the dimension $\hbar/m$, i.e., area over time. The equations of motion remain unchanged under the scaling if the time t is replaced by σt. In other words, all trajectories look the same along the parabola with constant η in the (E, κ) plane. The action for a trajectory can thus be decomposed into

$$S(k, \eta) = \hbar k \, \ell_{so}(\eta) \qquad \text{where} \qquad k = \sqrt{2mE}/\hbar \tag{30}$$

is the wave number. The function $\ell_{so}(\eta)$ has the dimension length and goes towards the geometrical length of the trajectory if $\eta \rightarrow \infty$, i.e. for vanishing spin-orbit interaction strength $\kappa \rightarrow 0$. In a realistic nuclear potential the coupling strength decreases with nucleon number A as $A^{-2/3}$ and a typical η value for a normally deformed actinide nucleus is $\eta \simeq 600$.

The scaling properties discussed above make it possible to analyse our numerical results by the Fourier transform method to be explained in the next subsection. All these considerations are true for arbitrary functional form of the spin-orbit potential. For the numerical calculations we choose it different from the mean field potential. One might argue that this is an unusual choice since in many nuclear physics calculations they are assumed to be the same. Firstly, a fit of the Woods-Saxon model to experimental levels shows that the two potentials can differ from each other [28]. Secondly and much more important, we are aiming at a model study in order to eludicate the role of spin in semiclassical approaches. At this stage of our investigations, we do not try to compete with full fledged quantitative quantum mechanical calculations. Hence we are convinced that our choice of the potentials which

make our model numerically feasible still gives the right picture. For the numerical calculations we choose

$$V_{so}(\vec{r}) \;=\; \left(\vec{r}^T C^2 \vec{r}\right)^{1/a_{so}} \;=\; |C\vec{r}|^{2/a_{so}} \quad . \tag{31}$$

For $a_{so} = 1$ this is a deformed harmonic oscillator. In this special case the "no name" part also becomes a deformed oscillator but in $\vec{e}_B$-space,

$$\lambda_{\pm}^{(1NN)} \;=\; \kappa\, \vec{e}_B^T\, C^2\, \vec{e}_B \quad . \tag{32}$$

If, in addition, the shape is spherical, the radial part of the spin-orbit interaction and the "no name" part are constants. Numerically, we also consider the case $a_{so} = 0.65$ besides $a_{so} = 1$.

2.5 Fourier Transform Technique

Trace formulas [15] provide a connection between the classical periodic orbits and the quantum mechanical density of energy levels. More precise, the trace of the semiclassical Green function gives approximately the level density $\rho(k)$ as a sum of the smooth Thomas-Fermi part $\rho_{TF}(k)$ plus a fluctuating part that is a sum over the periodic orbits

$$\rho(k) \;\simeq\; \rho_{TF}(k) + \sum_{\vec{m}} \sum_{n=1}^{\infty} A_{\vec{m},n}(k) \cos\left(\frac{S_{\vec{m},n}(k)}{\hbar} - \frac{n\pi}{2}\vec{\alpha}_{\vec{m}} \cdot \vec{m} + \frac{\pi}{4}\beta_{\vec{m}}\right) \quad . \tag{33}$$

where $k = \sqrt{2mE}/\hbar$ denotes the wave number. This particular sum is valid for integrable systems [17]. The vector $\vec{m}$ describes the topology of the periodic orbit. For example, a plane triangular orbit in a circular potential oscillates $m_r = 3$ times in the radial coordinate and $m_\varphi = 1$ times in the angular coordinate, thus $\vec{m} = (3,1)$ for this orbit. A plane pentagram like orbit has $\vec{m} = (5,2)$ and so on. For three dimensional orbits, $\vec{m}$ has of course three components. The index n gives the number of repetitions of the basic orbit characterized by $\vec{m}$. The components of the vector $\vec{\alpha}_{\vec{m}}$ are related to the number of conjugate points in the corresponding coordinates [32]. The number $\beta_{\vec{m}}$ comes from a stationary phase approximation and can take the values 0 and ± 1. Details about the amplitude $A_{\vec{m},n}(k)$ can be found in reference [17]. For our purposes, an important result is the factorization of the action in the case of cavities,

$$S_{\vec{m},n}(k) \;=\; \hbar k\, n\, \ell_{\vec{m}} \tag{34}$$

where $\ell_{\vec{m}}$ is the geometrical length of the basic periodic orbit.

A second connection between the periodic orbits and the level density suitable for cavities, is derived by taking a weighted Fourier transform [16] of the exact level density,

$$F(\ell) = \int_0^\infty \rho(k)\, k^q \exp(ik\ell)\, dk \quad . \tag{35}$$

The meaning of the weight function k^q will be explained below. The level density is a sum of δ-functions

$$\rho(k) = \sum_{\nu=1}^{\infty} \delta(E(k) - E(k_\nu)) = \frac{m}{\hbar^2} \sum_{\nu=1}^{\infty} \frac{1}{k_\nu} \delta(k - k_\nu) \quad , \tag{36}$$

this yields in equation (35)

$$F(\ell) = \frac{m}{\hbar^2} \sum_{\nu=1}^{\infty} k_\nu^{q-1} \exp(ik_\nu \ell) \quad . \tag{37}$$

In practice the integration in equation (35) must be terminated at a certain cutoff $k_{\max}$. An absolute minimum for a good resolution of the Fourier spectrum is to include levels up to $k_{\max} = 50/R_0$ which for spherical shape means up to about the first state with angular momentum $L = 44\hbar$. Obviously, the complex valued function $F(\ell)$ is strongly oscillating. If, however, the trace formula (33) is a good approximation, the dominant peaks of the modulus $|F(\ell)|$ will be according to equation (34) situated at points ℓ^* that are close to the lenghts $n\ell_{\vec{m}}$ of the periodic orbits. Furthermore, at the peak positions ℓ^* the argument $\Gamma(\ell) = \arg F(\ell)$ will approximately take the value $n\pi\vec{\alpha}_{\vec{m}} \cdot \vec{m}/2 - \pi\beta_{\vec{m}}/4$. The weight function k^q in equation (35) is introduced in order to compensate for the k dependence of the amplitude $A_{\vec{m},n}(k)$ in the trace formula (33).

Hence, in this paper, we will extract information about the classical periodic orbits from the Fourier transform of the level density calculated quantum mechanically and we will compare these findings with the calculation of periodic orbits using the classical equations of motion derived in the preceeding subsections. Due to the scaling property of our spin-orbit model discussed above we have effectively a cavity problem for a given fixed value of the parameter η. Consequently, the quantum mechanical eigenvalues used in the Fourier transform must lie along the parabola for constant η defined

by equation (29) in the (E, κ) plane. Since, for fixed η, equation (30) is of the same type as equation (34) we will find peak positions $\ell^*_{so}(\eta)$ for a given value of η. A further modification is the presence of the first order terms in the symplectic structure. According to our recipe discussed in subsection 2.3, we expect that the argument of $F(\ell)$ takes the value

$$\Gamma(\ell^*_{so}(\eta)) \simeq \frac{n\pi}{2}\vec{\alpha}_{\vec{m}} \cdot \vec{m} - \frac{\pi}{4}\beta_{\vec{m}} + \int \left(\lambda_{\pm}^{(1B)} + \lambda_{\pm}^{(1NN)}\right) dt \qquad (38)$$

at the peak positions where the time integration is along the periodic orbit. Berry's phase is purely geometrical, it is half the solid angle traced out by $\vec{e}_B$ on the unit sphere [11], and is therefore constant along the parabola in the (E,κ) plane with η constant. Moreover, the "no name" phase is also independent of the position on the parabola.

3 Classical and Quantal Results

The results of our classical and quantal numerical calculations are presented in subsections 3.1 and 3.2, respectively.

3.1 Classical Orbits

Defined by the initial conditions $(\vec{r}_0, \vec{p}_0)$, there are three geometrically different classes of trajectories and orbits: those that live in the circle in the equatorial (x, y) plane, those in the ellipse in an arbitrary fixed plane containing the symmetry axis, i.e. the z-axis, and all others that are truely three dimensional. We discuss them separately in the following.

3.1.1 Orbits in the Circle

For initial conditions with $(z_0, p_{z0}) = (0, 0)$ the equations of motion (26) restrict the trajectories to the circle in the equatorial plane. The adiabaticity assumption is obviously perfectly fulfilled since $\vec{L}$ and $\vec{e}_B$ are constants of motion pointing in the direction of $+\vec{e}_z$ or $-\vec{e}_z$.

It is very helpful to consider the case $a_{so} = 1$ which allows an easy direct calculation of the trajectories. Introducing $\vec{\rho} = (x, y)$ and $\vec{\pi} = (p_x, p_y)$ we can write

$$\dot{\vec{\rho}} = \frac{\vec{\pi}}{m} + \omega_c I \vec{\rho} \qquad \text{and} \qquad \dot{\vec{\pi}} = \omega_c I \vec{\pi} \qquad (39)$$

where we have defined the matrix

$$I = \begin{bmatrix} 0 & 1 \\ -1 & 0 \end{bmatrix} \qquad \text{and} \qquad \omega_c = 2\frac{\kappa}{R_\perp^2}\,\mathrm{sign}\,B_z \tag{40}$$

is a frequency. Note that $\mathrm{sign}\,B_z = \mathrm{sign}\,L_z$ is a constant of motion. The solution of the equations between two reflexions with initial conditions $(\vec{\rho}_0, \vec{\pi}_0)$ are simply straight lines seen from a rotating frame,

$$\vec{\rho}(t) = \exp(\omega_c t I)\left(\vec{\rho}_0 + \frac{\vec{\pi}_0}{m}t\right) \qquad \text{and} \qquad \vec{\pi}(t) = \exp(\omega_c t I)\,\vec{\pi}_0$$

$$\exp(\omega_c t I) = \begin{bmatrix} \cos\omega_c t & \sin\omega_c t \\ -\sin\omega_c t & \cos\omega_c t \end{bmatrix} \quad . \tag{41}$$

It is now possible to find the periodic orbits semianalytically. For a given η, the orbit characterized by the topology vector $\vec{m} = (m_r, m_\varphi)$ is defined by the angle $\varphi_{\vec{m}}$ appearing in the initial conditions in the form $\vec{\rho}_0 = (R_\perp, 0)$ and $\vec{\pi}_0 = \pi_0(-\cos\varphi_{\vec{m}}, \sin\varphi_{\vec{m}})$. The angle $\varphi_{\vec{m}}$, which can be restricted to lie between 0 and $\pi/2$, is the solution of the implicit equation

$$\frac{\cos\varphi_{\vec{m}}}{\sin\varphi_{\vec{m}} + (\mathrm{sign}\,\omega_c)\sqrt{\sin^2\varphi_{\vec{m}} + \mu^{2/3}\eta/2}} + \varphi_{\vec{m}} = \pi\left(\frac{1}{2} - \frac{m_\varphi}{m_r} + j\right) \tag{42}$$

where j is any integer, see the appendix for a derivation. Except for $\vec{m} = (2,1)$ there are for high η values two solutions for $\varphi_{\vec{m}}$, with $j = 0$, corresponding to the energetically favoured and unfavoured situation, respectively. For the motion along the diameter only the unfavoured case, i.e. negative ω_c, is possible. At extremely low η values more solutions with $j \neq 0$ for a given $\vec{m}$ are possible [33]. As an illustration we show the two triangle orbits $\vec{m} = (3,1)$ for $\eta = 189$ in figure 1. Observe that the unfavoured orbit is convex seen from outside and the favoured one concave.

3.1.2 Orbits in the Ellipse

All planes that contain the symmetry axis, i.e. the z-axis, are equivalent. Once defined by the initial conditions, the trajectories will leave neither of these ellipses. Contrary to the circle, neither $\vec{L}$ nor $\vec{e}_B$ are constants of motion.

It is again helpful to consider the case $a_{so} = 1$. We choose the (y, z) plane and define $\vec{\rho} = (y, z)$ and $\vec{\pi} = (p_y, p_z)$. The equations of motion (26) reduce to

$$\dot{\vec{\rho}} = \frac{\vec{\pi}}{m} + \omega_e I M \vec{\rho} \qquad \text{and} \qquad \dot{\vec{\pi}} = \omega_e M I \vec{\pi} \tag{43}$$

where we have introduced

$$\omega_e = 2\frac{\kappa}{R_\perp R_z} \operatorname{sign} B_x \qquad \text{and} \qquad M = \begin{bmatrix} \mu & 0 \\ 0 & \mu^{-1} \end{bmatrix} \quad . \tag{44}$$

Unless η is extremely low the classical motion falls into two categories. One type is bounded between the wall and an invisible inner ellipse, elliptic caustic [15], and we call this rotational like motion. The other type is bounded between the wall and two invisible hyperbolas, hyperbolic caustic, and is of vibrational type [19]. For the rotational type ω_e is a constant of motion. As an example of such motion two $\vec{m} = (4, 1)$ orbits are shown in figure 2 for $\mu = 1.6$ and $\eta = 212$. Since for these parameter values our system is not integrable, only isolated periodic orbits remain from the continous family of periodic orbits in the integrable case. In this and all other extreme adiabatic cases where the orientation of $\vec{e}_B$ is fixed the gauge potential vanishes and no Berry's phase is obtained. Thus noncanonical coordinates are not needed unless multiplicities of quantum levels or wave functions are of interest [14]. However, for vibrational like motion ω_e is not a constant of motion. For this type $\vec{e}_B$ happens to flip from $+\vec{e}_x$ to $-\vec{e}_x$, and the frequency ω_e changes sign. These sign changes are only possible if there is one point in between where the vector $\vec{B}$ is zero. Hence, according to our discussion above, the flips indicate precisely the mode conversion points. Since the relevant $\vec{B}$-space is reduced to the x-axis we are in the fortunate situation that the mode conversion points are really points in an one dimensional space. These special cirumstances make the orbits in the ellipse a beautiful and instructive example of mode conversion that we find worth to be discussed in more detail in the following. Between two mode conversion points occuring at times t_1 and t_2 and no reflexion at the boundary in between, equations (43) can be solved analytically,

$$\begin{aligned} \vec{\rho}(t) &= \exp(\omega_e(t - t_1) I M)\, \vec{\rho}(t_1) \\ &\qquad + \int_{t_1}^{t} \exp(\omega_e(t - t') I M)\, \exp(\omega_e(t' - t_1) M I)\, \frac{\vec{\pi}(t_1)}{m}\, dt' \\ \vec{\pi}(t) &= \exp(\omega_e(t - t_1) M I)\, \vec{\pi}(t_1) \end{aligned} \tag{45}$$

where the matrices involved are not simple rotations,

$$\begin{aligned} \exp(\omega_e t I M) &= \begin{bmatrix} \cos\omega_e t & -\mu^{-1}\sin\omega_e t \\ \mu\sin\omega_e t & \cos\omega_e t \end{bmatrix} \\ \exp(\omega_e t M I) &= \begin{bmatrix} \cos\omega_e t & -\mu\sin\omega_e t \\ \mu^{-1}\sin\omega_e t & \cos\omega_e t \end{bmatrix} . \end{aligned} \tag{46}$$

The integral in equation (45) yields combinations of trigonometric functions. At the time t_2, the sign of ω_e changes suddenly, thus, according to equation (43), the velocity $\dot{\vec{\rho}}$ changes direction by $2|\omega_e|IM\vec{\rho}$ producing strange kinks in the trajectories which are obviously unphysical. In this case the WKB treatment breaks down. Our special one dimensional situation however, allows an easy remedy for this problem: The $\vec{e}_B$ flips are equivalent to jumping from the Hamiltonian sheet for, say, spin up to that for spin down and vice versa. Hence, we simply have to get rid of sign B_x. Instead of the adiabatic Hamiltonian (25) we now introduce the diabatic Hamiltonian in the ellipse,

$$H_e^{\text{dia}}(\vec{\rho},\vec{\pi}) = \frac{\vec{\pi}^2}{2m} - \kappa B_x \tag{47}$$

by replacing $|B_x|$ with B_x. In our discussion for $a_{\text{so}} = 1$ the resulting equations of motion remain formally unchanged if we replace in equations (43) the frequency ω_e by

$$\omega_e^{\text{dia}} = 2\frac{\kappa}{R_\perp R_z} \tag{48}$$

which is obviously a constant of motion. Thus, under the same replacement, the solutions (45) are now valid everywhere except, of course, the reflexions at the boundary. The flips can now be interpreted as change of polarization. The new trajectories are kink free and physically reasonable, they are either fully diabatic or fully adiabatic depending on whether the spin flip occurs or not. As an example of a diabatically corrected orbit we show a member of the bowtie family in figure 3.

The impact of our diabatic correction procedure becomes most obvious in the changes of the organization of the phase space. Three Poincaré maps are plotted in figure 4 for a deformation $\mu = 1.6$ and a spin-orbit interaction with $\eta = 2121$ and $a_{\text{so}} = 1$. We use the familiar Birkhoff coordinates, s is the circumference and α the tangent angle after the reflexion at the boundary. The upper two maps are calculated using the adiabatic Hamiltonian (25) for

the two different signs of κ, the lower one is calculated using the diabatically corrected Hamiltonian (47). The latter map contains both the energetically favoured and unfavoured situations for α less and larger 90°, respectively. The two types of motion in the ellipse divide the phase space, the rotational like motion with elliptic caustic is confined to the upper and lower parts whereas the vibrational like motion with hyperbolic caustic appears in the middle. Obviously, the correction procedure changes the organization of the phase space drastically.

3.1.3 Three Dimensional Orbits

The remaining orbits are truely three dimensional. The equations of motion (26) can not be simplified since $\vec{e}_B$ is now moving continously. We are now generally in an intermediate situation between adiabatic and diabatic motion. Note that mode conversion does not take place since B_z is a constant of motion and non-zero. An estimate of the degree of adiabaticity is given by the quantity

$$\gamma = \frac{mR_0^2}{\hbar}\frac{\dot{B}_\perp}{B} \tag{49}$$

where $\dot{B}_\perp$ is the component of $\dot{\vec{B}}$ perpendicular to $\vec{B}$. The motion is expected to be adiabatic if always $\gamma \ll 1$ along the path while diabatic transitions most likely will occur whenever $\gamma \gg 1$.

In the cavity without spin-orbit coupling all non-planar periodic motion originates from bifurcations of the periodic orbits in the equatorial circle. The shortest one bifurcates from the $\vec{m} = (5,2)$ pentagram in the equatorial circle at $\mu = 1.618$. It performs one oscillation along the third axis and is consequentely denoted by $\vec{m} = (5,2,1)$. We show the two orbits, favoured and unfavoured, in figure 5 for the extremely deformed case $\mu = 2.0$ using a spin-orbit interaction with $\eta = 792$ and $a_{so} = 1$. As seen in figure 5(a), much of the pentagram structure remains in the equatorial plane. In figure 5(b) the projection onto the (x,z) plane is shown. The variation of the angle $\vartheta = \arccos(B_z/B)$ along the orbit is displayed in figure 6. The Berry's phase is, up to a sign, equal to half the solid angle traced out by $\vec{B}$ [11] and an estimate from figure 6 gives ±90°.

3.2 Fourier Transforms

In this section some typical Fourier transforms are presented and the information extracted from them is compared to the classical calculations. The quantum mechanical spectrum is obtained by introducing new stretched coordinates in which the ellipsoidal cavity is mapped onto a sphere whereas the kinetic energy becomes anisotropic [34]. In these new coordinates $\vec{B}$ is equal to the angular momentum times a radial function. The Hamiltonian is diagonalized for a set of κ values and we then interpolate to find the crossing of the energy levels with the parabola with η constant.

In figure 7 we show a Fourier transform for spherical shape $\mu = 1$, a strong spin orbit force $\eta = 189$ and for $a_{so} = 0.65$ as a thick line. For comparison we also plotted the Fourier transform for zero spin orbit force $\eta \rightarrow \infty$ as a thin line. The corresponding classical motion was described in subsection 3.1.1 since for spherical shape all motion is planar. Each peak with $m_r \geq 3$ for infinite η is split into two peaks at $\eta = 189$, one peak for each sign of κ in the Hamiltonian (25). Due to the cutoff of (37) this split is not seen for all periodic orbits in the shown ℓ_{so} interval. This limited resolution gives also a misleading picture of the relative importance of some of the periodic orbits. The two triangular orbits, shown in figure 1, are anyhow clearly resolved. In table 1 some values for the reduced action $\ell_{so}(\eta)$ and the phase $\Gamma(\ell_{so}(\eta))$ derived classically and from the Fourier transform are compared. To obtain the phase contribution from the "no name" part $\lambda_{\pm}^{(1NN)}$ the difference $\Gamma(\ell_{so}(\eta)) - \Gamma(\ell_{so}(\infty))$ should be taken. The discrepancy between the classical and quantal values for $\ell_{so}(\eta)$ is not larger with spin orbit force than without. When judging the agreement for the phase one should have in mind that it is a very sensitive quantity. Typically $\Delta\Gamma/\Delta\ell_{so} \simeq 14\pi/R_0$ in the $\ell_{so}(\eta)$ intervall considered. The dicrepancy between the classical and quantal values for the "no name" phase is just a few degrees except for the $\vec{m} = (5,1)$ orbit favoured by the spin-orbit force. In the deformed cavity this extreme adiabatic motion takes place in the equatorial circle and the ellipses containing the symmetry axis if the caustic is elliptic. We have resolved some of these peaks and found a good agreement with the classical values for $\ell_{so}(\eta)$ but we have not enough of reliable eigenenergies to provide a fair comparison for $\Gamma(\ell_{so}(\eta))$.

In figure 8 we investigate the diabatic orbits. The thin peak in figure 8 corresponds to zero spin-orbit force and is associated with a bowtie like family

of periodic orbits of which each member flips the orientation of $\vec{B}$ twice every period. This continous family of periodic orbits has in elliptical coordinates $\vec{m} = (4,1)$ and hyperbolic caustic. Observe that the peak is not split into two when the spin orbit force is turned on with $\eta = 212$ as shown by the thick line. From the discussion in subsection 3.1.2 we understand that the reason is that the spin does not follow the flips of $\vec{B}$ but instead switches polarization at each mode conversion point $\vec{B} = 0$. A classical orbit corresponding to this peak was shown in figure 3. The corresponding results in the table show that the diabatically corrected orbit is in good agreement with the quantal values. The reduction of the amplitude in figure 8 is due to the loss of symmetry for finite η.

An example of the intermediate situation is given in figure 9. The peak associated with the shortest non-planar orbit in the case of zero spin-orbit force is shown as thin line. It is the $\vec{m} = (5,2,1)$ orbit that bifurcates from the $\vec{m} = (5,2)$ pentagram in the equatorial plane at $\mu = 1.618$ as mentioned above. A very interesting question is now if one or two peaks will be seen in the Fourier transform when the spin-orbit coupling is turned on. From the discussion so far we draw the conclusion that adiabatic orbits cause a split into two peaks whereas diabatic orbits show up as one single peak. For the orbit in question, however, it is hard to tell what kind of behavior to expect since the quantity γ defined in equation (49) stays close to unity along the path. Thus, apriori it is unclear if the spin can follow $\vec{B}$, but as the solid curve calculated with $\eta = 792$ in figure 9 shows this is indeed the case. However, the agreement between the classical and quantal quantities is not of the same quality as for the other cases discussed above as follows from table 1. The difference between the $\ell_{\rm so}(\eta)$ values for the energetically unfavoured orbit is large and the discrepancy for the phase contribution that comes from the whole first order part $\lambda_{\pm}^{(1B)} + \lambda_{\pm}^{(1NN)}$ in the Hamiltonian is about 40° in both cases. A likely explanation is given in the discussion below. The orbits that correspond to the two thick peaks were shown in figure 5.

4 Summary and Discussion

We presented a semiclassical analysis of a system with spin-orbit interaction. In our approach, spin is not interpreted as the $SO(3)$ angular momentum of a top or gyroscope. We rather save the $SU(2)$ character of spin by approximat-

ing the multicomponent Schrödinger equation for the spinor wave function semiclassically. For this purpose we benefitted from the recent improvement of the WKB theory by Littlejohn and Flynn [12]. The diagonalization of the dispersion tensor gives two distinct Hamiltonians, one for each spin polarization. The effect of the spin on the orbital motion is an additional force and no extended phase space is needed. This is a great advantage of our approach compared to $SO(3)$ like pictures. Another helpful feature is that our method allows planar motion which, as shown by our numerical results, influences the quantum spectra strongly. This does not occur generally in $SO(3)$ like models due to the occurence of a precessional motion [8]. The classical equations of motion are an adiabatic approximation because of the use of WKB techniques. Motivated by nuclear physics we studied a deformed system with axial symmetry. In this model, the adiabaticity assumption means that the vector $\vec{B}$ appearing in the spin-orbit interaction has to move slowly. We chose a cavity with ideally reflecting boundary as mean field potential in order to furnish our model system with a scaling property. This implies enormous simplifications for our numerical calculations. We chose the spin-orbit potential different from the mean field. This might be unusual from the nuclear physice viewpoint although it is known that the potentials can differ from each other. However, we feel free in our choice of potential since we are not aiming at quantitative nuclear structure calculations but rather at a general study of spin in semiclassical theories. Our results convince us that our model gives the right physical insight.

To extract classical information from quantum mechanical spectra we were guided by the trace formula and used Fourier transform technique. Our numerical calculations show that the WKB approximation for the spin-orbit coupling works as well as the standard scalar WKB method if the motion of the vector $\vec{B}$ is sufficiently slow. A large part of our Fourier spectra consists of peaks associated with planar orbits. They belong to the adiabatic limit or, if mode conversions occur, the diabatic limit. We were able to construct a diabatic correction of the classical Hamiltonian in the case of the latter and the numerical calculations for the bowtie orbit confirm our considerations. From our Fourier transforms we draw the conclusion that as the spin-orbit interaction is turned on a peak corresponding to an adiabatic orbit generally splits up into two whereas a peak associated with a diabatic orbit stays on its position almost unchanged. In the case of the three dimensional orbits

we are in an intermediate regime between adiabatic and diabatic motion, so the situation is less clear. The non-planar orbit we investigated is, despite that γ in (49) is about unity, surprisingly of the adiabatic type. However, the phase is about 40° off.

From the semiclassical theory follows that for zero spin-orbit force, i.e. $\eta \rightarrow \infty$ no Berry's phase should be included but for any finite η it must be. This transition is abrupt but our experience from similar situations tells us that a gradual transition takes place in the quantal case. Here, we have in mind, for example, the transition from spherical to deformed potential where, in the evaluation of traces formulas, the stationary phase approximation gives rise to abrupt phase changes. Hence, we conclude that there is a region of the parameter η were semiclassical mechanics can not work well. The finding that 40° are missing for both phase values is most probably due to the fact that Berry's phase is not fully developed at our parameter value $\eta = 792$. To clarify this situation, further and detailed numerical calculations have to be performed. From the results available now for the intermediate situation we believe that only very close to a mode conversion, $\vec{B} = 0$, jumps between the Hamiltonian sheets corresponding to different spin polarizations will occur. All these considerations allow the conclusion that our recipe, i.e. the simplyfing assumptions to interprete the zeroth order WKB approximation $\lambda_{\pm}^{(0)} + E$ as classical Hamiltonian for the canonical equations of motion whereas the full first order contribution $\lambda_{\pm}^{(1B)} + \lambda_{\pm}^{(1NN)}$ is included in the symplectic form, turned out to be very resonable. Hence, despite some technical difficulties with the three dimensional orbits, it seems that our method gives an easier handle on spin problems than extended phase space approaches of the $SO(3)$ type [8, 9].

From a nuclear physics point of view the results show that the effect of the spin-orbit force at large deformations, compared to spherical shape, is reduced since the orbits with hyperbolic caustic are insensitive to a change of the coupling strength. This effect is even more pronounced in the case of the anisotropic harmonic oscillator where all planar motion within the ellipse is of this type. Our Hamiltonian (25) is similar to the cranking Hamiltonian investigated in reference [33] and therefore we, contrary to reference [9], claim that a realistic spin-orbit force is only slightly chaos producing. If the mean field gives rise to strongly chaotic motion most orbits will be of the diabatic type. Our study shows that the superdeformed potential, where the

adiabatic, intermediate and diabatic motion are all important, is an unique system to study spin properties. At a further stage our investigations might be important for concrete nuclear physics applications, for example for the understanding of new effects in rotating superdeformed nuclei [27].

In our opinion the basic notion is the coupled wave fields, two in our case and four in the Dirac equation. The Pauli matrices provide the most general coupling of the wave fields. By means of a diagonalization procedure we can work with two Hamiltonians separately. As for the outcome of Stern-Gerlach experiments, these Hamiltonians can not be understood from a picture of the particle as a spinning magnet. However, as already pointed out in reference [13] these two subsystems, or three if mode conversion takes place, give rise to interference effects in the eigenfunctions. It is at this stage gyroscope like considerations become useful. For semiclassical calculations it is, as demonstrated in this paper, most convenient to work with the underlying discrete subsystems.

Appendix

The "no name" contribution is calculated in appendix A. The implicit equation (42) is derived in appendix B.

A Evaluation of the "No Name" Contribution

First we calculate the Poisson-brackets of the components of the vector $\vec{B}$,

$$\{B_i, B_j\} = \varepsilon_{ijk} \left(\vec{B} \cdot \frac{\partial}{\partial \vec{r}}\right) \frac{\partial V_{so}}{\partial x_k} = \varepsilon_{ijk} \left(\frac{\partial^2 V_{so}}{\partial \vec{r} \partial \vec{r}^T} \vec{B}\right)_k \quad . \tag{50}$$

The left hand side can be considered as the element of a dyadic matrix, thus we have in an index free notation

$$\{\vec{B}, \vec{B}^T\} = \vec{J} \cdot \left(\frac{\partial^2 V_{so}}{\partial \vec{r} \partial \vec{r}^T} \vec{B}\right) \quad , \tag{51}$$

where the components of the vector $\vec{J}$ are the generators of the group $O(3)$, i.e. 3×3 matrices. These Poisson bracket relations are obviously related to those of the angular momentum which are recovered if the spin orbit potential

$V_{so}(\vec{r})$ is an isotropic harmonic oscillator. The next step is to calculate the Poisson-brackets of two functions $F = F(\vec{B})$ and $G = G(\vec{B})$ that depend on $\vec{B}$, but not explicitly on the phase space coordinates $(\vec{r}, \vec{p})$,

$$\begin{aligned}
\{F(\vec{B}), G(\vec{B})\} &= \frac{\partial \vec{B}^T}{\partial \vec{r}} \frac{\partial F}{\partial \vec{B}} \cdot \frac{\partial \vec{B}^T}{\partial \vec{p}} \frac{\partial G}{\partial \vec{B}} - \frac{\partial \vec{B}^T}{\partial \vec{r}} \frac{\partial G}{\partial \vec{B}} \cdot \frac{\partial \vec{B}^T}{\partial \vec{p}} \frac{\partial F}{\partial \vec{B}} \\
&= \frac{\partial F}{\partial \vec{B}^T} \left(\frac{\partial \vec{B}}{\partial \vec{r}^T} \frac{\partial \vec{B}^T}{\partial \vec{p}} - \frac{\partial \vec{B}}{\partial \vec{p}^T} \frac{\partial \vec{B}^T}{\partial \vec{r}} \right) \frac{\partial G}{\partial \vec{B}} \\
&= \frac{\partial F}{\partial \vec{B}^T} \{\vec{B}, \vec{B}^T\} \frac{\partial G}{\partial \vec{B}} \quad . \qquad (52)
\end{aligned}$$

Since the vector $\vec{J}$ generates the vector product we find after inserting equation (51) into equation (52)

$$\{F(\vec{B}), G(\vec{B})\} = \left(\frac{\partial G}{\partial \vec{B}} \times \frac{\partial^2 V_{so}}{\partial \vec{r} \partial \vec{r}^T} \vec{B} \right) \cdot \frac{\partial F}{\partial \vec{B}} = \left(\frac{\partial F}{\partial \vec{B}} \times \frac{\partial G}{\partial \vec{B}} \right) \cdot \frac{\partial^2 V_{so}}{\partial \vec{r} \partial \vec{r}^T} \vec{B} \quad . \qquad (53)$$

This result can now be used for the evaluation of the "no name" contribution. In an index free notation, the second of equations (15) can be rewritten as

$$\begin{aligned}
\lambda_{\pm}^{(1NN)} &= \frac{i}{2} \operatorname{tr} \left(D - \lambda_{\pm}^{(0)} 1_2 \right) \{\tau^{(\pm)}, \tau^{(\pm)\dagger}\} \\
&= -i \frac{\kappa}{2} \operatorname{tr} \begin{bmatrix} B_z \pm B & B_- \\ B_+ & -B_z \pm B \end{bmatrix} \{\tau^{(\pm)}, \tau^{(\pm)\dagger}\} \quad . \qquad (54)
\end{aligned}$$

In order to calculate the Poisson brackets of the polarization vectors with the help of equation (53) we use the spherical coordinates introduced in subsection 2.2. Hence we have $B_z = B \cos\vartheta$ and $B_\pm = B \exp(\pm i\varphi) \sin\vartheta$, the gradient operator is given by

$$\frac{\partial}{\partial \vec{B}} = \vec{e}_B \frac{\partial}{\partial B} + \frac{\vec{e}_\vartheta}{B} \frac{\partial}{\partial \vartheta} + \frac{\vec{e}_\varphi}{B \sin\vartheta} \frac{\partial}{\partial \varphi} \quad . \qquad (55)$$

For the polarization vectors we choose the north standard gauge

$$\begin{aligned}
\tau^{(-)} &= \begin{bmatrix} \cos(\vartheta/2) \\ \exp(+i\varphi) \sin(\vartheta/2) \end{bmatrix} \\
\tau^{(+)} &= \begin{bmatrix} -\exp(-i\varphi) \sin(\vartheta/2) \\ \cos(\vartheta/2) \end{bmatrix} \quad . \qquad (56)
\end{aligned}$$

It is obvious that the vector products of the gradients of the components of these vectors must be parallel to $\vec{e}_B$. A direct calculation yields

$$\{\tau^{(+)}, \tau^{(+)\dagger}\} = \frac{i}{4B} \begin{bmatrix} 2 & \exp(-i\varphi)\tan(\vartheta/2) \\ \exp(+i\varphi)\tan(\vartheta/2) & 0 \end{bmatrix} \vec{e}_B^T \frac{\partial^2 V_{\rm so}}{\partial\vec{r}\,\partial\vec{r}^T} \vec{e}_B \tag{57}$$

and similar for $\tau^{(-)}$. Collecting everything and evaluating the trace in equation (54) gives the desired result

$$\lambda_{\pm}^{(1\mathrm{NN})} = \frac{\kappa}{2} \vec{e}_B^T \frac{\partial^2 V_{\rm so}}{\partial\vec{r}\,\partial\vec{r}^T} \vec{e}_B \tag{58}$$

which is independent of the polarization index.

B Derivation of Equation (42)

Starting from, for example, $\vec{\rho}_0 = (R_\perp, 0)$ the trajectory will hit the boundary again at the time t_R and at the point $\vec{\rho}(t_R)$ with the property $R_\perp^2 = \vec{\rho}^{\,2}(t_R)$. Using equation (41) and writing $\vec{\pi}_0 = \pi_0(-\cos\varphi_{\vec{m}}, \sin\varphi_{\vec{m}})$, where we can restrict ourselves to the regime $0 \leq \varphi_{\vec{m}} \leq \pi/2$, we find

$$t_R = 2\frac{mR_\perp}{\pi_0}\cos\varphi_{\vec{m}} \quad . \tag{59}$$

Moreover, for a periodic orbit with topology vector $\vec{m} = (m_r, m_\varphi)$ it is geometrically easy to see that

$$\vec{\rho}_0 \cdot \vec{\rho}(t_R) = R_\perp^2 \cos(2\pi m_\varphi/m_r) \quad . \tag{60}$$

This yields, again with the help of equation (41), after some algebra the equation

$$\frac{1}{u}\cos\varphi_{\vec{m}} + \varphi_{\vec{m}} = \pi\left(\frac{1}{2} - \frac{m_\varphi}{m_r} + j\right) \qquad \text{where} \qquad u = \frac{\pi_0}{m\omega_c R_\perp} \tag{61}$$

and j is an integer. We now have to express the dimensionless parameter u as a function of η. From definition (29) we find

$$\eta = \frac{R_0^4}{mR_z^2\kappa^2}\left(\frac{\pi_0^2}{2m} - \kappa B_z \mathrm{sign}\, B_z\right) = 2\mu^{-2/3}\left(u^2 - 2u\sin\varphi_{\vec{m}}\right) \tag{62}$$

which can be solved for u. Hence, we arrive at

$$\frac{\cos\varphi_{\vec{m}}}{\sin\varphi_{\vec{m}} \pm \sqrt{\sin^2\varphi_{\vec{m}} + \mu^{2/3}\eta/2}} + \varphi_{\vec{m}} = \pi\left(\frac{1}{2} - \frac{m_\varphi}{m_r} + j\right) \tag{63}$$

with the plus and minus sign for orbits favoured and unfavoured in energy by the spin-orbit coupling, respectively. For very small η values solutions with $j \neq 0$ are possible [33].

Acknowledgements

We are grateful to William Flynn, Robert Littlejohn and Vladek Swiatecki for many stimulating discussions. TG also benefitted from fruitful conversations with Robert Arvieu and Petr Rozmej during the conference on quantum chaos in Copenhagen in spring 1991. HF was supported by a postdoctoral fellowship from the Swedish Natural Science Research Council. He also wants to express his gratitude to the Nuclear Science Division for their hospitality and support.

References

[1] J.D. Bjorken and S.D. Drell, **Relativistic Quantum Mechanics**, McGraw-Hill, New York, 1964

[2] H. Mathur, Phys. Rev. Lett. **67** (1991) 3325

[3] M. Mayer, Phys. Rev. **78** (1950) 16; O. Haxel, J. Jensen and H.E. Suess, Z. Phys. **128** (1950) 295

[4] A. Bohr and B. Mottelson, **Nuclear Structure**, vol. I and II, Benjamin, New York, 1969 and 1975

[5] G.E. Brown, W. Weise, G. Baym and J. Speth, Comm. Nuc. Part. Phys. **17** (1987) 39

[6] J.S. Bell, J. de Phys. Colloque C2 suppl. au numero 3 **42** (1981) 42; reprinted in **Speakable and Unspeakable in Quantum Mechanics**, Cambridge University Press, Cambridge, 1987

[7] H.C. Corben, **Classical and Quantum Theories of Spinning Particles**, Holden-Day, San Francisco, 1968

[8] R. Arvieu, P. Rozmej and M. Ploszajczak, **Phase Space Structure of Simple Nuclear Models** in **PREDEAL summer school: New Trends in Theoretical and Experimental Physics**, World Scientific (to be published)

[9] B. Milek and J. Reif, Z. Phys. **A339** (1991) 231

[10] K. Yabana and H. Horiuchi, Prog. Theor. Phys. **75** (1986) 592

[11] M. Berry, Proc. Roy. Soc. London **A392** (1984) 45; H. Kuratsuji and S. Iida, Prog. Theor. Phys. **74** (1985) 439; F. Wilczek and A. Shapere, **Geometrical Phases in Physics**, World Scientific, Singapore, 1989

[12] R.G. Littlejohn and W.G. Flynn, Phys. Rev. **A44** (1991) 5239

[13] R. Balian and C. Bloch, Ann. Phys. (NY) **85** (1974) 514

[14] R.G. Littlejohn and W. Flynn, submitted to Phys. Rev.

[15] M. C. Gutzwiller, **Chaos in Classical and Quantum Mechanics**, Springer-Verlag, New York, 1990

[16] R. Balian and C. Bloch, Ann. Phys. (NY) **69** (1972) 76

[17] M. V. Berry and M. Tabor, Proc. R. Soc. London **A349** (1976) 101

[18] V. M. Strutinsky, A. G. Magner, S. R. Ofengenden and T. Düssing, Z. Phys. **A283** (1977) 269

[19] H. Frisk, Nucl. Phys. **A511** (1990) 309

[20] M. V. Berry and J. P. Keating, J. Phys. **A23** (1990) 4839; M. Sieber and F. Steiner, Phys. Rev. Lett. **67** (1991) 1941; G. Tanner, P. Scherer, E. B. Bogomolny, B. Eckhardt and D. Wintgen, Phys. Rev. Lett. **67** (1991) 2410

[21] E. Bogomolny, Physica **D31** (1988) 169

[22] H. Frisk, Phys. Scripta **43** (1991) 545

[23] R.P. Feynman and A.R. Hibbs, **Quantum Mechanics and Path Integrals**, McGraw-Hill, New York, 1965

[24] L. Schulman, **Techniques and Applications of Path Integration**, Wiley, New York, 1981

[25] A. M. Polyakov, Mod. Phys. Lett. **A3** (1988) 325; T. Jaroszewicz and P.S. Kursepa, Ann. Phys. (NY) **210** (1991) 255

[26] P. Batenburg and A.M.J. Schakel, Mod. Phys. Lett. **A4** (1989) 1355

[27] F.S. Stephens et al., Phys. Rev. Lett. **65** (1990) 301

[28] J. Dudek and T. Werner, J. Phys. **G4** (1978) 1543

[29] R.G. Littlejohn, J. Math. Phys. **31** (1990) 2952

[30] S.W. McDonald, Phys. Rep. **158** (1988) 337

[31] S. Åberg, H. Flocard and W. Nazarewicz, Annu. Rev. Nucl. Part. Sci. **40** (1990) 439; R.V.F. Janssens and T.L. Khoo, Annu. Rev. Nucl. Part. Sci. **41** (1991) 321

[32] S.C. Creagh, J.M. Robbins and R.G. Littlejohn, Phys. Rev. **A42**(1990) 1907

[33] H. Frisk and R. Arvieu, J. Phys. **A22** (1989) 1765

[34] Y. Ayant and R. Arvieu, J. Phys. **A20** (1987) 1115

Table 1: Reduced actions $\ell_{so}(\eta)$ and phases $\Gamma(\ell_{so}(\eta))$ for five periodic orbits, associated with peaks in the Fourier transforms. The classical and quantal results are given. In every column the values for zero spin-orbit force are on the left and those for finite spin-orbit force on the right. The first three orbits are planar, the triangle, the rectangle and the pentagon. They appear in two versions for the energetically unfavoured and favoured situation, corresponding to upper and lower row, respectively. The fourth orbit is the planar bowtie in the ellipse with hyperbolic caustic, it is diabatic and hence does not split up. The last orbit is the non-planar one that bifurcates from the pentagram in the equatorial circle. It is of the intermediate type but does split up. This orbit is the only one where Berry's phase contributes.

$\vec{m}$	$\ell_{so}(\eta)$				$\Gamma(\ell_{so}(\eta))$			
	classical		quantal		classical		quantal	
(3,1)		4.879		4.882		243		256
	5.196		5.201		225		241	
		5.438		5.441		240		250
(4,1)		5.121		5.123		157		166
	5.657		5.658		135		147	
		6.129		6.135		154		171
(5,1)		5.218				70		
	5.878		5.874		45		48	
		6.512		6.520		67		85
$(4,1)_h$	7.010	7.002	7.007	7.006	180	199	190	203
(5,2,1)		7.847		7.883		19		95
	7.979		7.987		90		124	
		8.109		8.097		188		185

Figure 1: The two triangular orbits in the equatorial circle, $\mu = 1$, for a strong spin-orbit interaction with $\eta = 189$ and $a_{so} = 0.65$. The thick and the thin solid lines show the orbits favoured and unfavoured in energy, respectively. The first is concave from outside, the second convex.

Figure 2: Two rectangular orbits in the ellipse, $\mu = 1.6$, for a spin-orbit interaction with $\eta = 212$ and $a_{so} = 1.0$. The thick and the thin solid lines show the orbits favoured and unfavoured in energy, respectively. Here and in the following figures, the ellipses are rotated by 90°, hence the z axis is horizontal.

Figure 3: An diabatically corrected bowtie like orbit which is member of a family in the ellipse, $\mu = 1.6$, for a spin-orbit interaction with $\eta = 212$ and $a_{so} = 1.0$.

Figure 4: Poincaré maps in Birkhoff coordinates for the planar motion in the ellipse, $\mu = 1.6$ employing a spin-orbit interaction with $\eta = 212$ and $a_{so} == 1$. The top and the middle figure are calculated using the adiabatic Hamiltonian (25) in the unfavoured and favoured case, respectively. The bottom figure is calculated using the diabatically corrected Hamiltonian (47). Observe the drastic differences.

Figure 5: The shortest non-planar orbit, here shown for $\eta = 792$, $\mu = 2.0$ and $a_{so} = 1.0$. The thick and the thin solid lines correspond to the situation favoured and unfavoured in energy, respectively. (a) Projected onto the equatorial (x, y) plane. (b) Projected onto the (x, z) plane.

Figure 6: The motion of the vector $\vec{B}$ for the orbit shown in figure 5, the thick and the thin solid lines correspond to situation favoured and unfavoured in energy, respectively. The angle $\vartheta = \arccos(B_z/B)$ is plotted versus the normalized time t/T where T is the total period.

Figure 7: Fourier transforms of the level density for a spherical cavity without spin-orbit interaction and with a strong spin-orbit interaction, $\eta = 189$ and $a_{so} = 0.65$, as thin and thick lines, respectively. All levels below $k = 86.6/R_0$ are included and the exponent in equation (35) is $q = -1/2$. The abscissa is the reduced action $\ell_{so}(\eta)$ which goes towards the geometrical length when $\eta \to \infty$. In the thick peak to the right all orbits with $m_r \geq 6$ and $m_\varphi = 1$ are merged together. The thin line shows that the each peak is splitted into two, one for each spin polarization, when the spin-orbit interaction is turned on. The subscripts u and f denote orbits unfavoured and favoured in energy by the spin-orbit force, respectively. Observe that $(4,1)_u$ and $(7,1)_f$ are not fully resolved.

Figure 8: Fourier transforms for a superdeformed potential, $\mu = 1.6$ without spin-orbit interaction and with a realistic spin-orbit interaction, $\eta = 212$ and $a_{so} = 1$, as thin and thick lines, respectively. All levels below $k = 50/R_0$ are included and the exponent in equation (35) is $q = 0$. The thin peak comes from a bowtie like family of planar periodic orbits with hyperbolic caustic for which the vector $\vec{B}$ changes orientation 180° twice a period. This process is too fast for the spin which then changes polarization. Thus the thick line does not show two peaks. The peak position remains essentially fixed but the height and phase of the Fourier transforms change.

Figure 9: Fourier transforms for a superdeformed potential, $\mu = 2.0$ without spin-orbit interaction and with a spin-orbit interaction, $\eta = 792$ and $a_{so} = 1$, as thin and thick lines, respectively. The exponent in equation (35) is $q = 0$. The thin peak is due to a non-planar orbit for which the motion of the vector $\vec{B}$ is intermediate between the cases shown in figures 2 and 3. This orbit bifurcates from the pentagram orbit in the equatorial plane at $\mu \simeq 1.6$. Despite that $\gamma \simeq 1$ two peaks are seen for the thick line when the spin-orbit interaction is turned-on. This shows that indeed the spin can follow the vector $\vec{B}$.

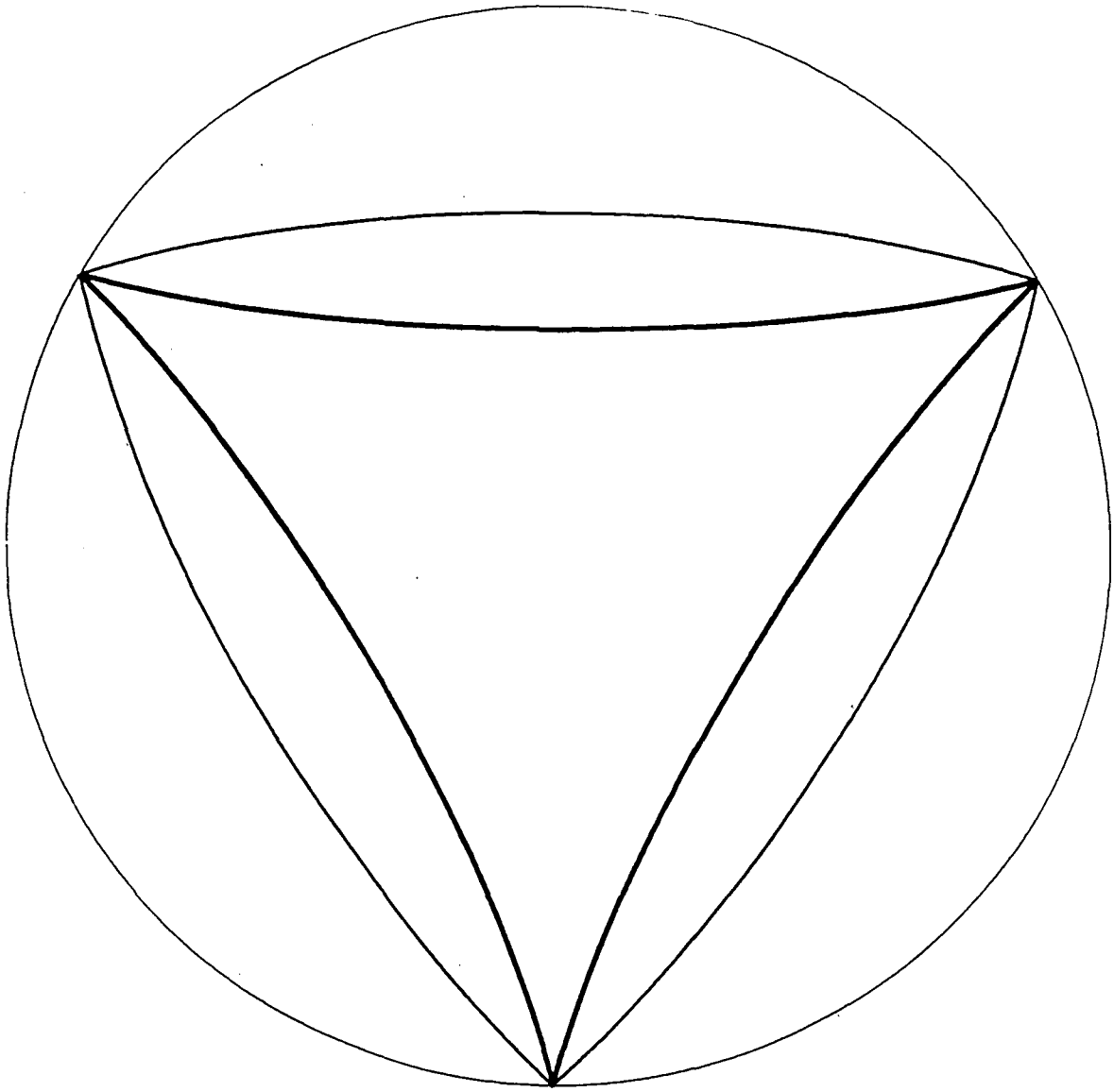

XBL 924-603

Figure 1

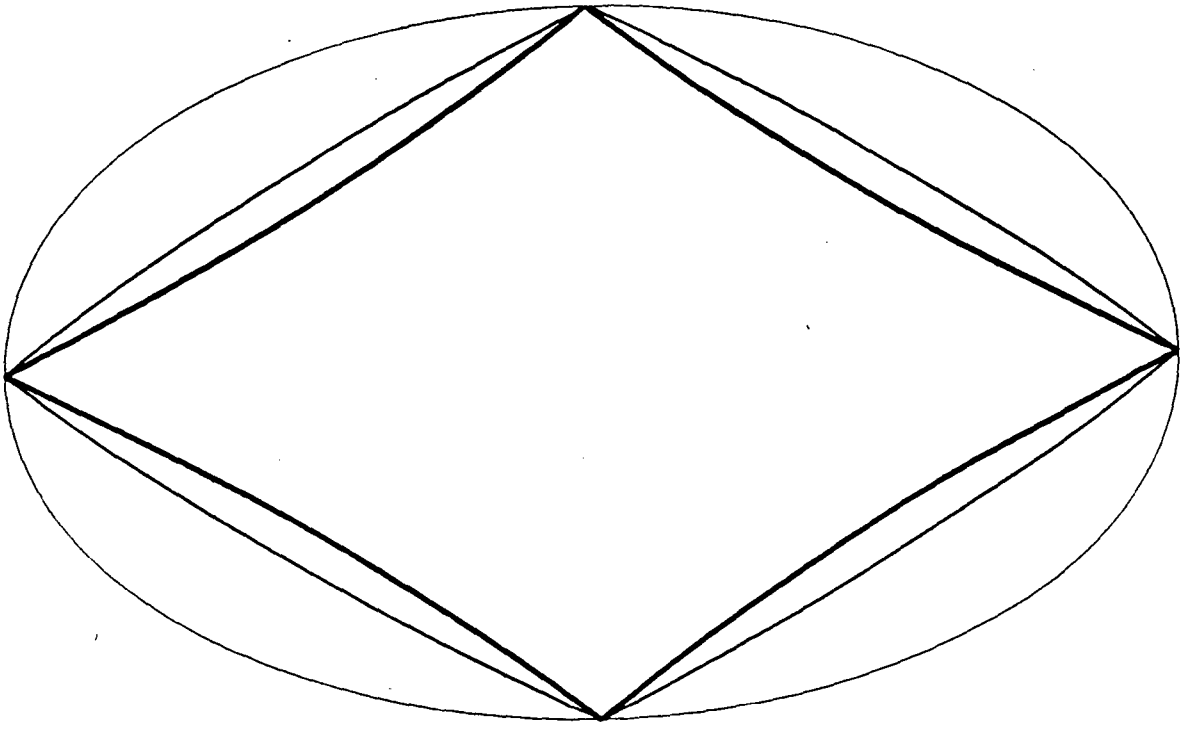

XBL 924-604

Figure 2

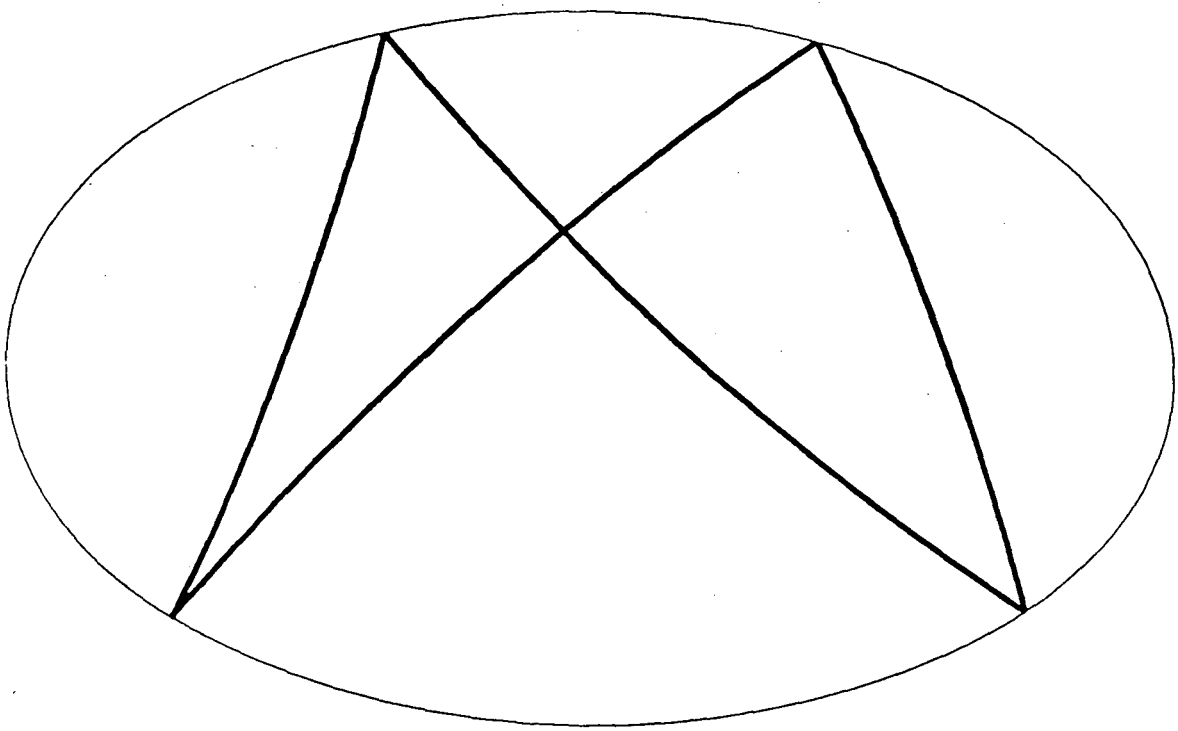

XBL 924-605

Figure 3

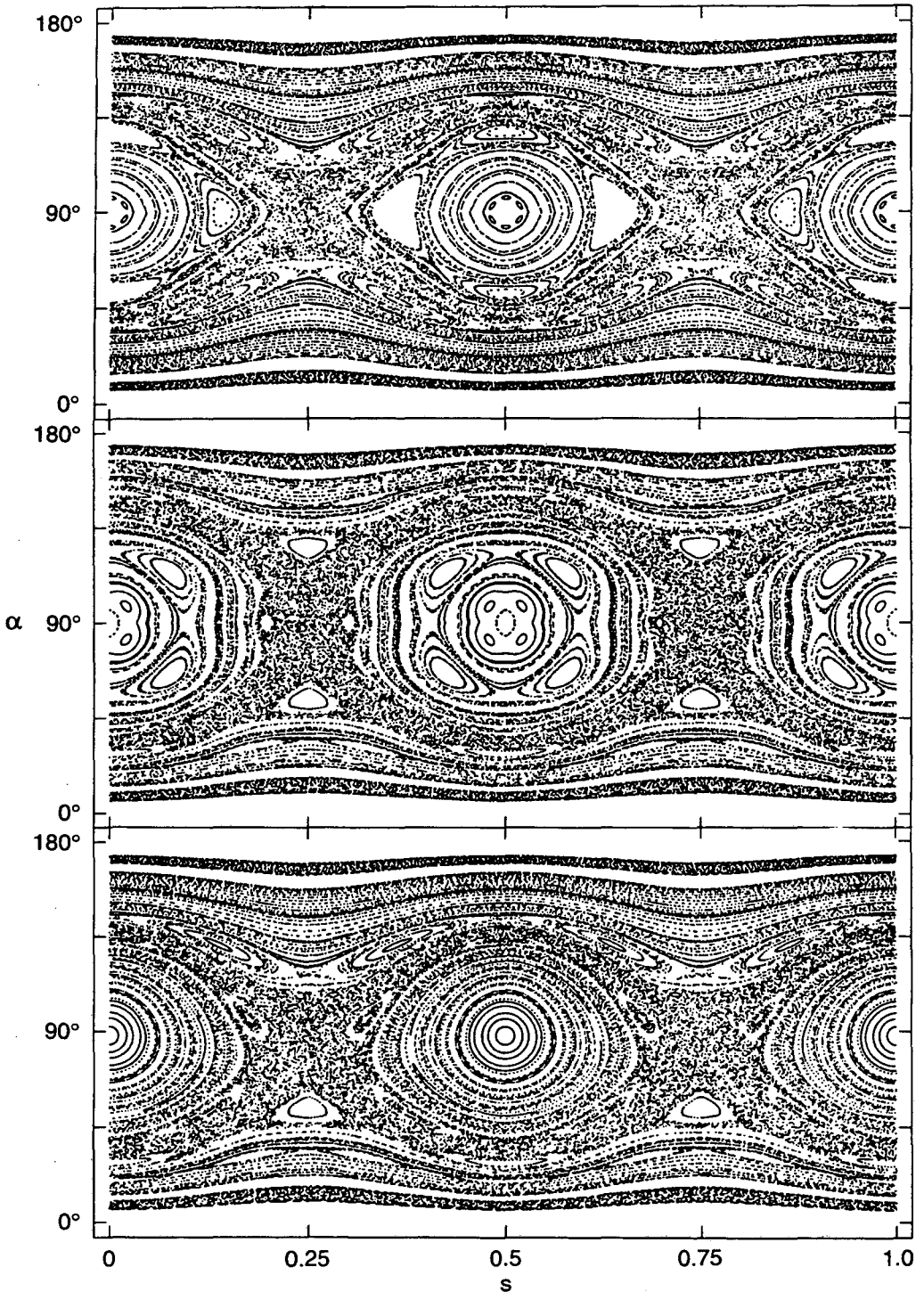

XBL923-6057

Figure 4

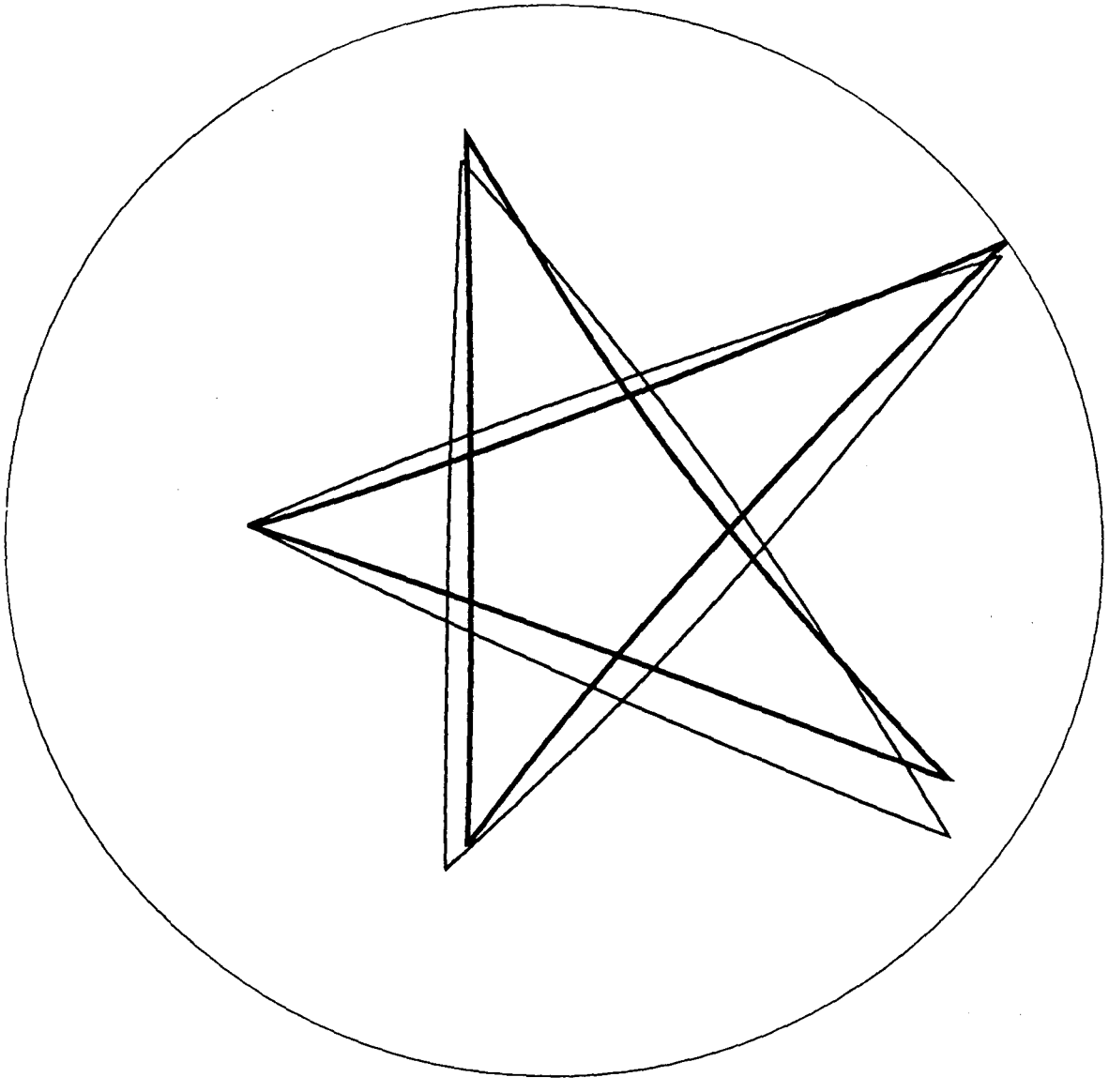

XBL 924-606

Figure 5a

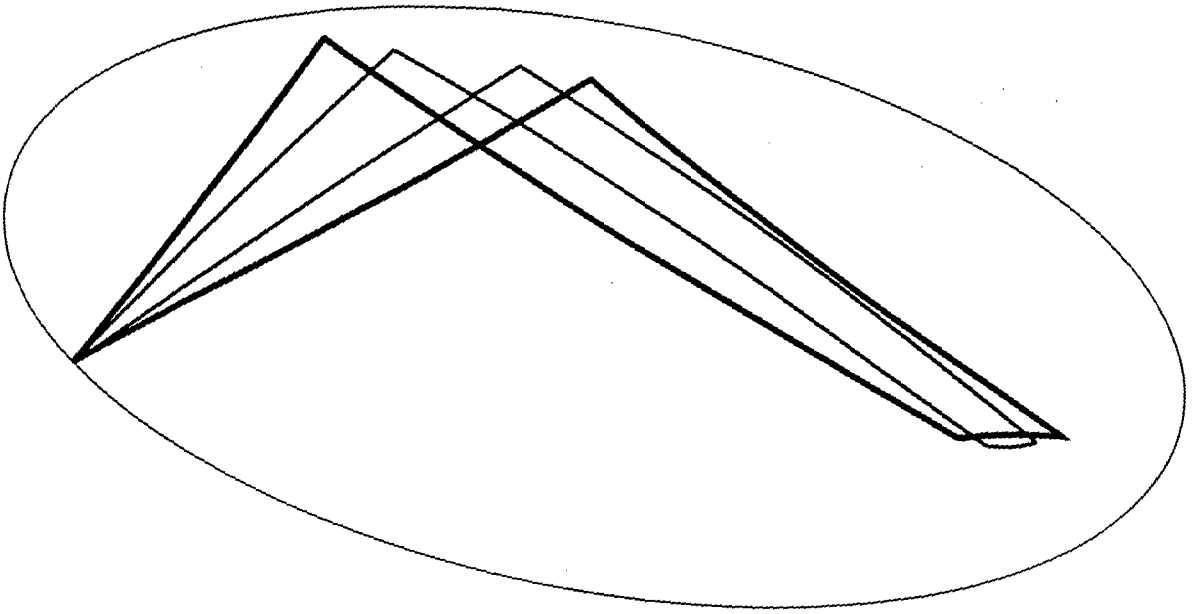

XBL 924-607

Figure 5b

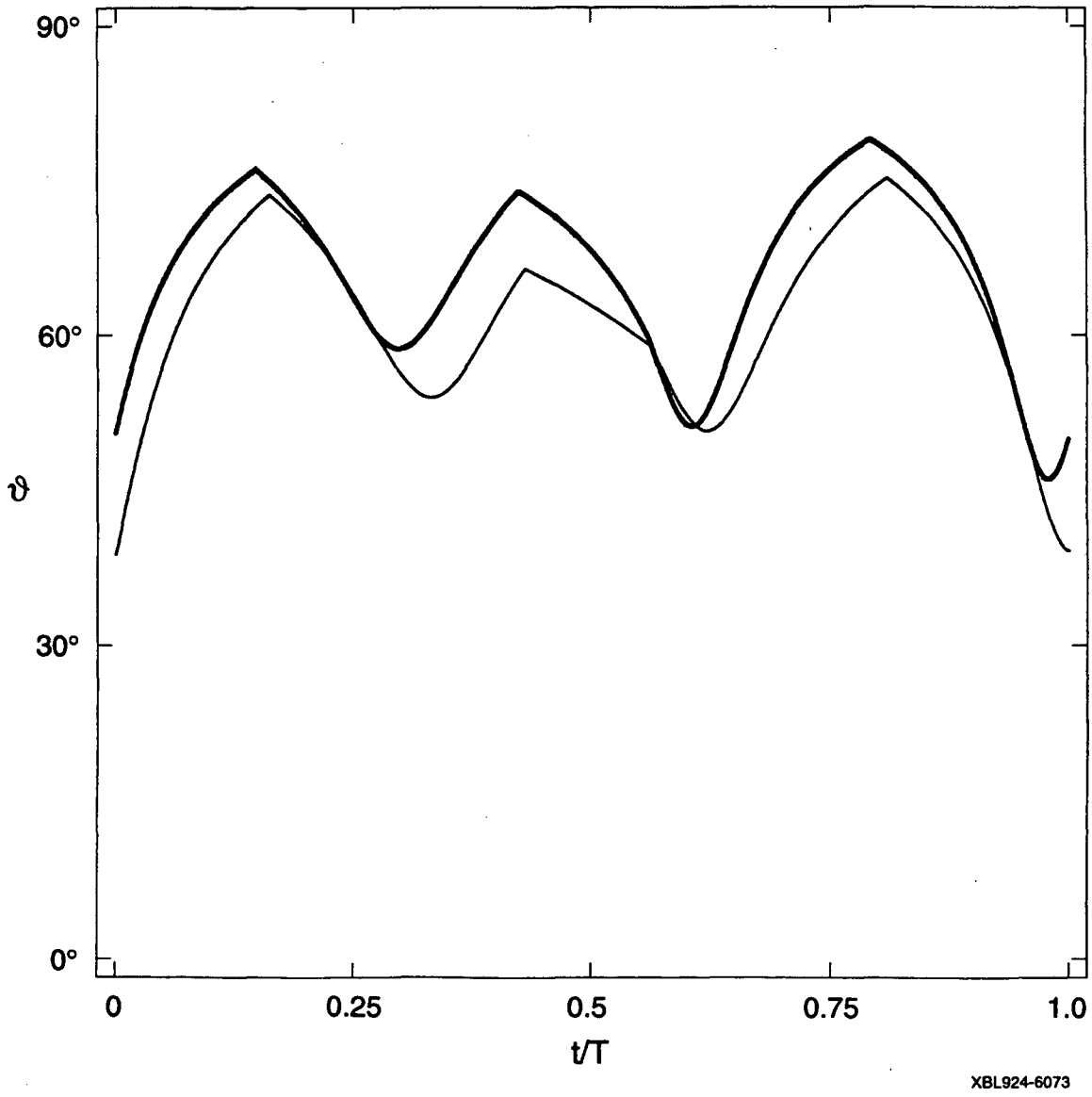

Figure 6

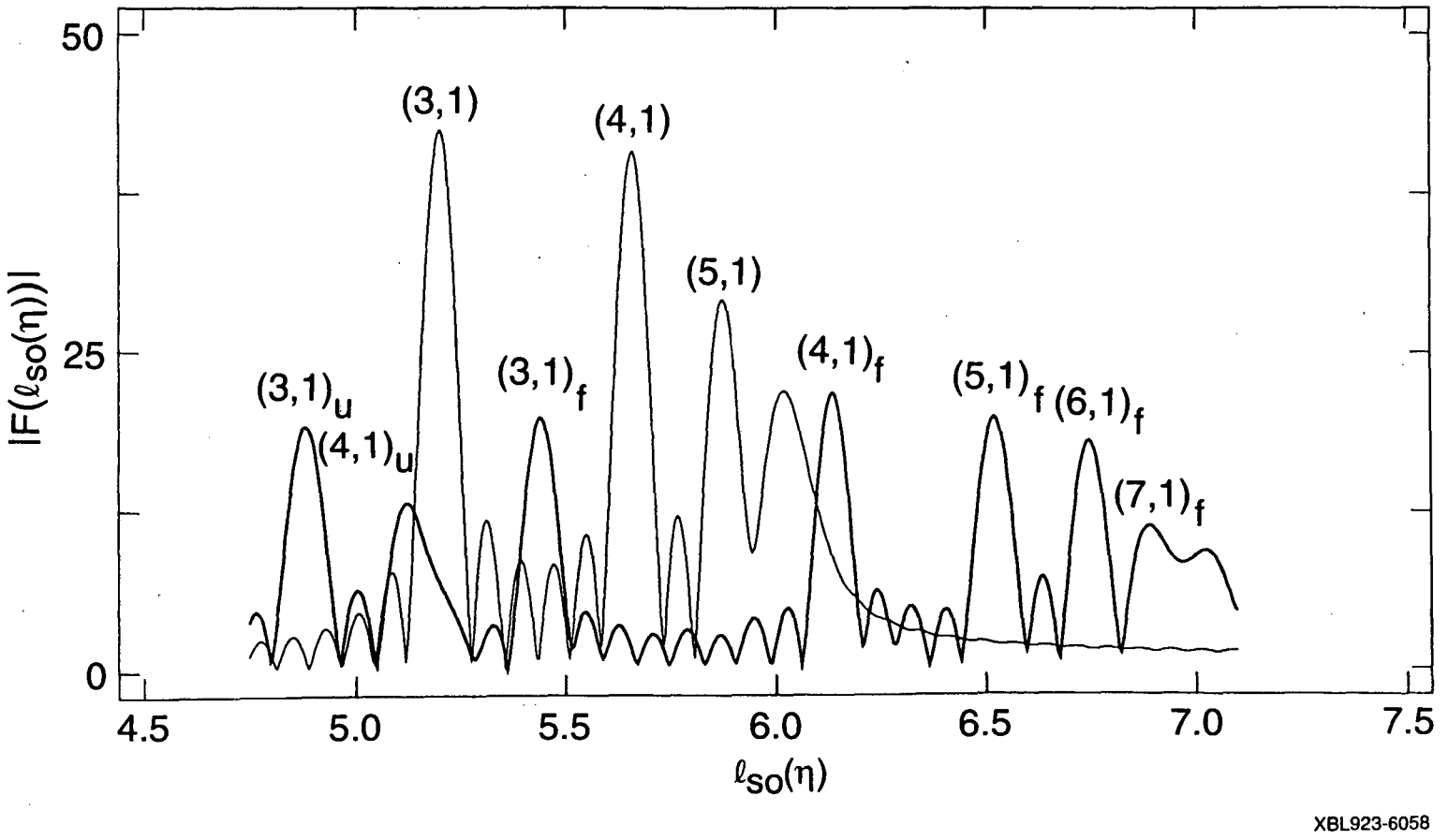
50
25
0
|F(ℓso(η))|
(3,1)
(4,1)
(5,1)
(3,1)u
(4,1)u
(3,1)f
(4,1)f
(5,1)f
(6,1)f
(7,1)f
4.5
5.0
5.5
6.0
6.5
7.0
7.5
ℓso(η)
XBL923-6058

Figure 7

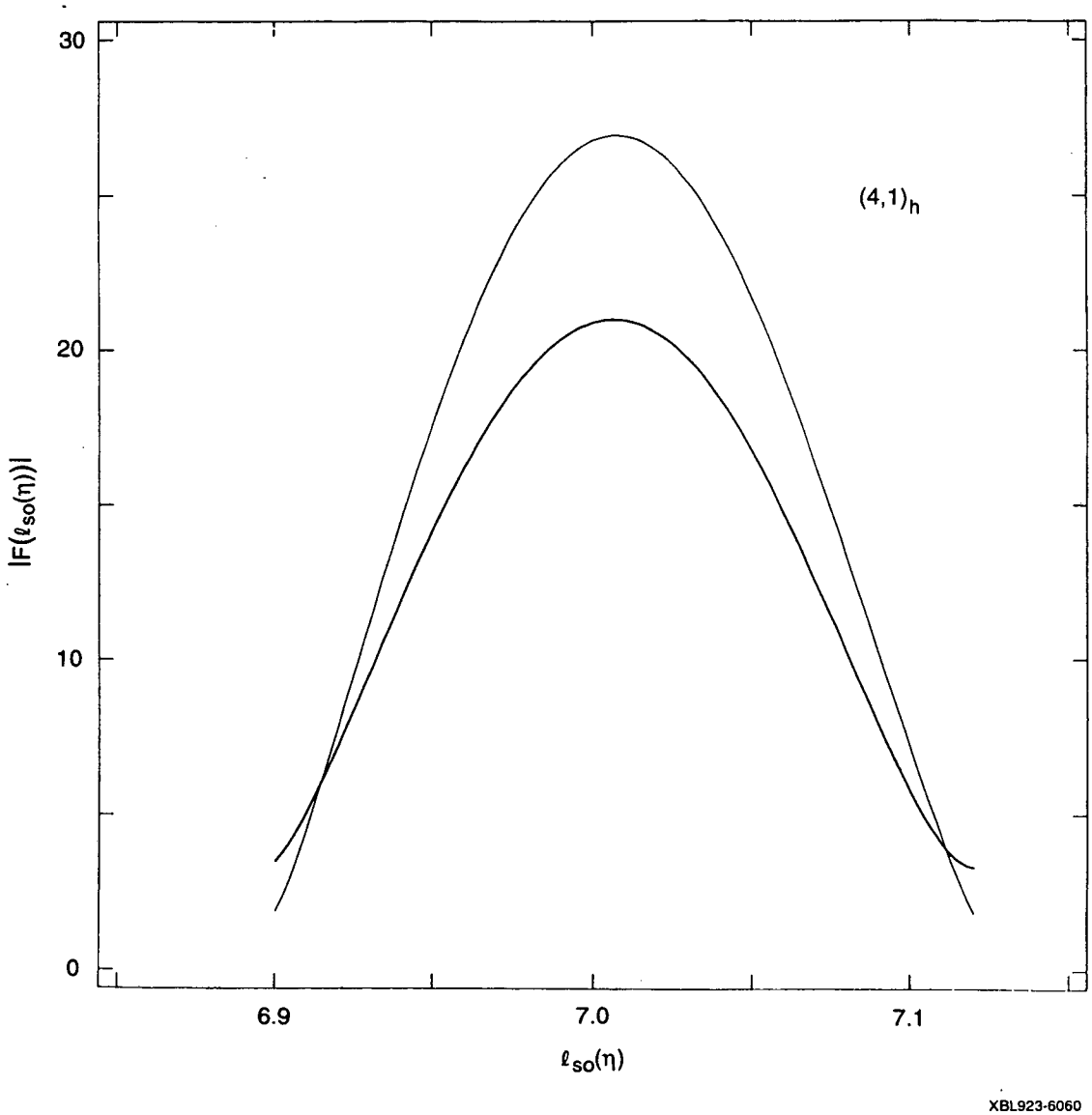

Figure 8

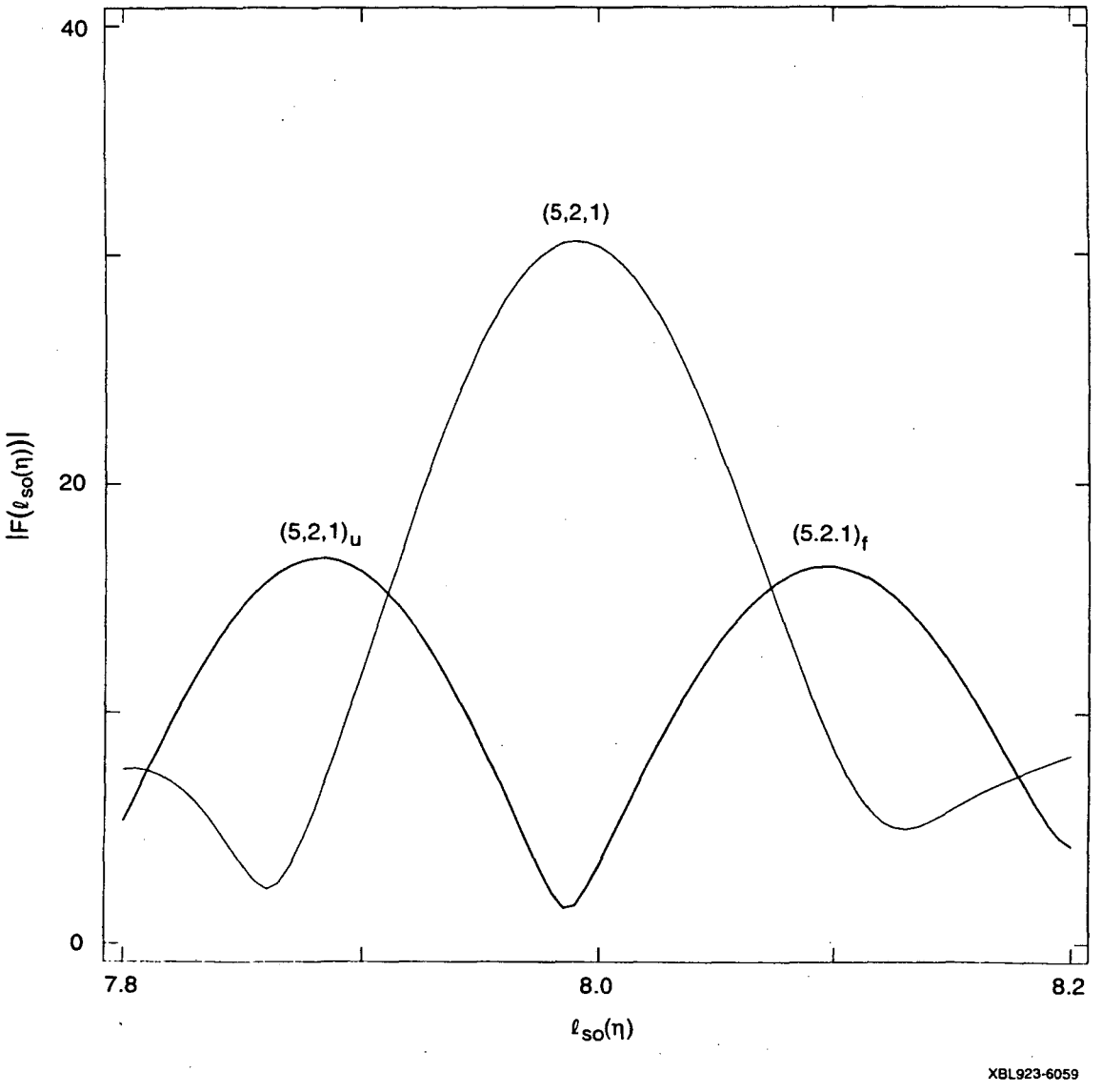

Figure 9

LAWRENCE BERKELEY LABORATORY
UNIVERSITY OF CALIFORNIA
TECHNICAL INFORMATION DEPARTMENT
BERKELEY, CALIFORNIA 94720